Table 1 Neurotransmitter levels in prefrontal cortex, striatum and nucleus accumbens of wild-type and *Slitrk1*-knockout mice

	Prefrontal cortex		*Striatum*		*Nucleus accumbens*	
	WT	*KO*	*WT*	*KO*	*WT*	*KO*
NE	4210.3 ± 115.4	4681.4 ± 132.9*	74.1 ± 15.0	77.3 ± 13.5	2785.0 ± 581.8	3578.6 ± 485.1
DA	2344.7 ± 383.8	2340.1 ± 307.2	99 532.2 ± 7476.2	93 077.7 ± 2658.7	59 585.6 ± 4392.2	60 868.4 ± 3379.1
5-HT	2833.5 ± 232.8	2941.8 ± 178.2	2286.6 ± 194.6	2163.6 ± 73.4	3892.1 ± 360.6	4557.3 ± 330.7
DOPAC	776.4 ± 56.5	768.4 ± 50.0	21 514.1 ± 1881.1	17 079.2 ± 1814.2	15 644.7 ± 943.7	14 946.5 ± 1055.8
MHPG	678.7 ± 30.5	853.3 ± 131.4	457.4 ± 30.8	535.2 ± 78.8	636.3 ± 46.5	836.4 ± 101.1**
HVA	1899.4 ± 172.5	2406.8 ± 300.9	12 359.5 ± 638.3	12 382.0 ± 657.8	8824.8 ± 642.5	10 356.9 ± 919.4
5-HIAA	3545.3 ± 126.7	3680.3 ± 269.1	2037.9 ± 125.6	2149.6 ± 170.3	2575.1 ± 189.6	3265.3 ± 246.4**
3-MT	305.0 ± 33.1	278.6 ± 25.4	7883.1 ± 622.9	6730.0 ± 196.0	5208.9 ± 381.7	5100.1 ± 416.0
Ach	NA	NA	2805.5 ± 476.2	2401.7 ± 270.7	2262.5 ± 266.1	2218.4 ± 151.5
CH	NA	NA	210 569.8 ± 12 868.8	177 557.3 ± 6655.4*	123 583.5 ± 5619.3	123 616.8 ± 7070.0

Abbreviations: WT, wild type; KO, knockout; 3-MT, 3-methoxytyramine; 5-HIAA, 5-hydroxyindoleacetic acid; 5-HT, serotonin; HVA, homovanillic acid; Ach, acetylcholine; CH, choline; DA, dopamine; DOPAC, 3,4-dihydroxyphenylacetic acid; MHPG, 3-methoxy-4-hydroxyphenylglycol; NA, not available; NE, norepinephrine.
*$P<0.05$; **$P<0.01$ (Student's *t*-test).
Values are presented as mean ± s.e.m. (pg/μg protein) of six animals.

test, whereas the drug had little effect on wild-type mice (Figures 4a and b). In contrast, clonidine treatment did not alter the locomotor activity of either wild-type or *Slitrk1*-deficient mice (Figure 4c).

Discussion

In the present study, we developed *Slitrk1*-knockout mice and analyzed their behavioral and neurochemical phenotypes. *Slitrk1*-deficient mice exhibited elevated anxiety-like behavior in elevated plus-maze test and increased immobility time in forced swimming and tail suspension tests. The brains of *Slitrk1*-deficient mice had increased levels of norepinephrine and MHPG, and administration of clonidine, an α2-adrenergic agonist, attenuated the anxiety-like behavior of *Slitrk1*-knockout mice.

The results of the present study strongly suggest the involvement of norepinephrine mechanisms in the elevated anxiety-like behavior of *Slitrk1*-knockout mice. Recently, Hu *et al.* revealed that norepinephrine is involved in the formation of emotional memory by regulating AMPA-receptor trafficking, and injection of epinephrine enhanced the formation of fear-conditioned contextual memory.[23] The result also suggests that the increased norepinephrine content of *Slitrk1*-deficient mice contributes to the increased freezing in the contextual fear-conditioning experiment (Figure 3e). Slitrk1 protein is not abundant in the pons and medulla oblongata, which contain noradrenergic neuronal cell bodies, including those in the locus coeruleus.[24] Indeed, *Slitrk1*-deficient mice lacked overt abnormalities in noradrenergic neurons of the locus coeruleus (Supplementary Figure S5). However, Slitrk1 is produced abundantly in brain areas receiving projections of noradrenergic neurons, such as cerebral cortex, hippocampus, amygdala, thalamus and hypothalamus (Figure 1).[24] Although the molecular properties of Slitrk1 have not been clarified yet, our present results indicate that it contributes to noradrenergic neurotransmission.

In this study, *Slitrk1*-deficient mice displayed not only elevated anxiety-like behavior but also depression-like behavioral abnormality, characterized by increased immobility time in forced swimming and tail suspension tests (Figures 3g and h). The monoamine-deficiency hypothesis postulates that depression is caused by the deficiency in serotonin and/or norepinephrine neurotransmission,[25] and compounds that can inhibit reuptake of norepinephrine or serotonin are widely used as antidepressants. Increased levels of norepinephrine and MHPG were observed in *Slitrk1*-deficient brain, suggesting an altered status of the noradrenergic neurotransmission. Although further analyses are needed to clarify the causes and effects of the transmitter content abnormality, preclinical and clinical evidence suggests a relationship between increased noradrenergic neurotransmission and symptoms associated with stress and anxiety.[24,26] Considering the anxiety-like behavior in the *Slitrk1*-deficient mice, the altered noradrenergic transmission may be involved in the appearance of depression-like behavior.

As the noradrenergic system, the cholinergic system is involved in fear and anxiety. Systemic injection of mice with muscarinic antagonists increases anxiety, whereas administration of nicotinic agonists decreases anxiety, in the elevated plus-maze test.[27,28] Single injections of nicotine also decrease the freezing response of rats in the contextual fear-conditioning test.[29] Furthermore, clinical evidence from patients with Alzheimer's disease also supports a relationship between the cholinergic system and anxiety. Alzheimer's disease is associated with decreased cholinergic levels, and roughly 33% of patients with Alzheimer's syndrome also suffer from

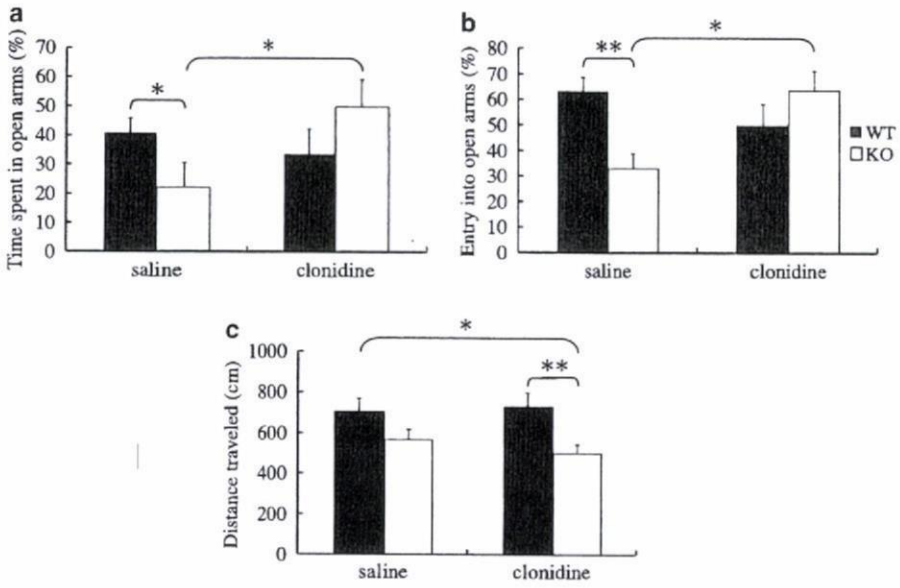

Figure 4 Administration of clonidine attenuated the elevated anxiety-like behavior of *Slitrk1*-knockout mice in the elevated plus-maze test. Injection of clonidine increased the percentage of time spent in open arms ($U=14$, $P<0.05$) (**a**) and entries into open arms in *Slitrk1*-deficient mice ($U=10.5$, $P<0.05$) (**b**), whereas the drug had no effect on locomotor activity (**c**). $^{*}P<0.05$, $^{**}P<0.01$; Student's *t*-test (parametric data), Mann–Whitney's *U*-test (percentage data); and mean ± s.e.m.; $n=10$ (saline) or 11 (clonidine) for wild-type mice and $n=8$ (saline) or 9 (clonidine) for knockout mice.

anxiety disorders. More importantly, treatment with acetylcholinesterase inhibitors has decreased anxiety in these patients.[30] Therefore, the decreased choline and acetylcholine levels of *Slitrk1*-deficient mice may be important in their increased anxiety-like behavior.

Mutations in *SLITRK1* are found in patients with TS or TTM.[7,8,31] These two syndromes are believed to belong to the OCD spectrum of diseases. However, *Slitrk1*-deficient mice did not display any abnormalities in the marble-burying behavior test (Supplementary Figure S4f), a paradigm used to detect OCD symptoms as well as anxiety-like behavior in animals.[32,33] Although the behavioral phenotypes of *Slitrk1*-knockout mice are not fully consistent with those of TS patients, these mice display some of the phenomena of TS patients and may yield insight into the pathogenesis of TS. Tic disorders including TS often are associated with anxiety disorders, mood disorders including major depression and phobias.[34,35] In the present study, *Slitrk1*-deficient mice displayed elevated anxiety-like behavior that was attenuated by the administration of clonidine, a drug frequently used to treat patients with TS. These results suggest possible association of the elevated anxiety-like behavior induced by the dysfunction of Slitrk1 and the symptoms of TS.

In agreement with the behavioral abnormalities of *Slitrk1*-deficient mice, *SLITRK1* mutation in humans seems to be associated with anxiety- or mood-related disorders. For example, one proband diagnosed with TS and ADHD demonstrated a frameshift mutation in *SLITRK1*; the patient's mother, who had TTM, had the same mutation.[7] In addition, a patient with TTM and *SLITRK1* mutation also had mild anxiety and a history of depression; her mother, who carried the mutation, had a history of depression, low self-esteem, and a fear of heights.[8] In the other case, a patient with TTM and *SLITRK1* mutation had no other clinically significant mood, anxiety or behavior problems; however, her father, who was a mutation carrier, was formally diagnosed with TTM and social phobia and a history of bulimia, and his sister, who was not available for genetic testing, had also been diagnosed with TTM and had a history of anxiety and depressive disorders.[8] Combining these findings with the results of present study, we hypothesize that *SLITRK1* may be involved in the control of anxiety, fear and mood, which are closely related to TS and TTM.

Human *SLITRK1* is located on 13q31.1, a region linked strongly with panic disorder, schizophrenia, bipolar disorder and recurrent depressive disorder.[36–39] Clinical studies suggest a relationship between norepinephrine and behaviors of anxiety and fear, as well as alterations in noradrenergic function in patients with psychiatric disorders related to anxiety and stress, panic disorder and posttraumatic stress disorder.[26,40,41] Further analysis of *Slitrk1*-deficient mice will be beneficial for understanding the pathogenesis of TS and other related neuropsychiatric diseases.

Acknowledgments

We thank Dr Tadafumi Kato and Dr Takeo Yoshikawa (RIKEN BSI) for their critical comments on the paper, Dr Mika Tanaka and Ms Chieko Nishioka for their assistance in generating *Slitrk1*-knockout mice, Ms Chihiro Homma for her assistance in behavioral analysis and Mr Masaki Kumai (Support Unit for Animal Experiments, RIKEN BSI) for his help in

generating the anti-Slitrk1 antibody. This study was supported by RIKEN BSI funds and the Japan Society for the Promotion of Science.

References

1 Aruga J, Mikoshiba K. Identification and characterization of Slitrk, a novel neuronal transmembrane protein family controlling neurite outgrowth. *Mol Cell Neurosci* 2003; **24**: 117–129.
2 Aruga J, Yokota N, Mikoshiba K. Human SLITRK family genes: genomic organization and expression profiling in normal brain and brain tumor tissue. *Gene* 2003; **315**: 87–94.
3 Kobe B, Deisenhofer J. Proteins with leucine-rich repeats. *Curr Opin Struct Biol* 1995; **5**: 409–416.
4 Brose K, Tessier-Lavigne M. Slit proteins: key regulators of axon guidance, axonal branching, and cell migration. *Curr Opin Neurobiol* 2000; **10**: 95–102.
5 Patapoutian A, Reichardt LF. Trk receptors: mediators of neurotrophin action. *Curr Opin Neurobiol* 2001; **11**: 272–280.
6 Chen Y, Aulia S, Li L, Tang BL. AMIGO and friends: an emerging family of brain-enriched, neuronal growth modulating, type I transmembrane proteins with leucine-rich repeats (LRR) and cell adhesion molecule motifs. *Brain Res Brain Res Rev* 2006; **51**: 265–274.
7 Abelson JF, Kwan KY, O'Roak BJ, Baek DY, Stillman AA, Morgan TM *et al*. Sequence variants in SLITRK1 are associated with Tourette's syndrome. *Science* 2005; **310**: 317–320.
8 Züchner S, Cuccaro ML, Tran-Viet KN, Cope H, Krishnan RR, Pericak-Vance MA *et al*. SLITRK1 mutations in trichotillomania. *Mol Psychiatry* 2006; **11**: 887–889.
9 Leckman JF. Tourette's syndrome. *Lancet* 2002; **360**: 1577–1586.
10 Robertson MM, Cavanna AE. The Gilles de la Tourette syndrome: a principal component factor analytic study of a large pedigree. *Psychiatr Genet* 2007; **17**: 143–152.
11 Hautmann G, Hercogova J, Lotti T. Trichotillomania. *J Am Acad Dermatol* 2002; **46**: 807–821; quiz 822–806.
12 Inoue T, Hatayama M, Tohmonda T, Itohara S, Aruga J, Mikoshiba K. Mouse Zic5 deficiency results in neural tube defects and hypoplasia of cephalic neural crest derivatives. *Dev Biol* 2004; **270**: 146–162.
13 Sakai K, Miyazaki J. A transgenic mouse line that retains Cre recombinase activity in mature oocytes irrespective of the cre transgene transmission. *Biochem Biophys Res Commun* 1997; **237**: 318–324.
14 Sadakata T, Washida M, Iwayama Y, Shoji S, Sato Y, Ohkura T *et al*. Autistic-like phenotypes in Cadps2-knockout mice and aberrant CADPS2 splicing in autistic patients. *J Clin Invest* 2007; **117**: 931–943.
15 Satoh Y, Endo S, Ikeda T, Yamada K, Ito M, Kuroki M *et al*. Extracellular signal-regulated kinase 2 (ERK2) knockdown mice show deficits in long-term memory; ERK2 has a specific function in learning and memory. *J Neurosci* 2007; **27**: 10765–10776.
16 Tang YP, Shimizu E, Dube GR, Rampon C, Kerchner GA, Zhuo M *et al*. Genetic enhancement of learning and memory in mice. *Nature* 1999; **401**: 63–69.
17 Porsolt RD, Bertin A, Blavet N, Deniel M, Jalfre M. Immobility induced by forced swimming in rats: effects of agents which modify central catecholamine and serotonin activity. *Eur J Pharmacol* 1979; **57**: 201–210.
18 Wesolowska A, Nikiforuk A. Effects of the brain-penetrant and selective 5-HT6 receptor antagonist SB-399885 in animal models of anxiety and depression. *Neuropharmacology* 2007; **52**: 1274–1283.
19 Silva RH, Kameda SR, Carvalho RC, Takatsu-Coleman AL, Niigaki ST, Abilio VC *et al*. Anxiogenic effect of sleep deprivation in the elevated plus-maze test in mice. *Psychopharmacology (Berl)* 2004; **176**: 115–122.
20 Pringsheim T, Davenport WJ, Lang A. Tics. *Curr Opin Neurol* 2003; **16**: 523–527.
21 Robertson MM. Attention deficit hyperactivity disorder, tics and Tourette's syndrome: the relationship and treatment implications. A commentary. *Eur Child Adolesc Psychiatry* 2006; **15**: 1–11.
22 Schlicker E, Göthert M. Interactions between the presynaptic α2-autoreceptor and presynaptic inhibitory heteroreceptors on noradrenergic neurones. *Brain Res Bull* 1998; **47**: 129–132.
23 Hu H, Real E, Takamiya K, Kang MG, Ledoux J, Huganir RL *et al*. Emotion enhances learning via norepinephrine regulation of AMPA-receptor trafficking. *Cell* 2007; **131**: 160–173.
24 Bremner JD, Krystal JH, Southwick SM, Charney DS. Noradrenergic mechanisms in stress and anxiety. I. Preclinical studies. *Synapse* 1996; **23**: 28–38.
25 Belmaker RH, Agam G. Major depressive disorder. *N Engl J Med* 2008; **358**: 55–68.
26 Bremner JD, Krystal JH, Southwick SM, Charney DS. Noradrenergic mechanisms in stress and anxiety. II. Clinical studies. *Synapse* 1996; **23**: 39–51.
27 Rodgers RJ, Cole JC. Effects of scopolamine and its quaternary analogue in the murine elevated plus-maze test of anxiety. *Behav Pharmacol* 1995; **6**: 283–289.
28 Brioni JD, O'Neill AB, Kim DJ, Decker MW. Nicotinic receptor agonists exhibit anxiolytic-like effects on the elevated plus-maze test. *Eur J Pharmacol* 1993; **238**: 1–8.
29 Szyndler J, Sienkiewicz-Jarosz H, Maciejak P, Siemiatkowski M, Rokicki D, Czlonkowska AI *et al*. The anxiolytic-like effect of nicotine undergoes rapid tolerance in a model of contextual fear conditioning in rats. *Pharmacol Biochem Behav* 2001; **69**: 511–518.
30 Weiner MF, Svetlik D, Risser RC. What depressive symptoms are reported in Alzheimer's patients? *Int J Geriatr Psychiatry* 1997; **12**: 648–652.
31 Grados MA, Walkup JT. A new gene for Tourette's syndrome: a window into causal mechanisms? *Trends Genet* 2006; **22**: 291–293.
32 Takeuchi H, Yatsugi S, Yamaguchi T. Effect of YM992, a novel antidepressant with selective serotonin re-uptake inhibitory and 5-HT 2A receptor antagonistic activity, on a marble-burying behavior test as an obsessive-compulsive disorder model. *Jpn J Pharmacol* 2002; **90**: 197–200.
33 Matsushita M, Egashira N, Harada S, Okuno R, Mishima K, Iwasaki K *et al*. Perospirone, a novel antipsychotic drug, inhibits marble-burying behavior via 5-HT1A receptor in mice: implications for obsessive-compulsive disorder. *J Pharmacol Sci* 2005; **99**: 154–159.
34 Kurlan R, Como PG, Miller B, Palumbo D, Deeley C, Andresen EM *et al*. The behavioral spectrum of tic disorders: a community-based study. *Neurology* 2002; **59**: 414–420.
35 Robertson MM. Mood disorders and Gilles de la Tourette's syndrome: an update on prevalence, etiology, comorbidity, clinical associations, and implications. *J Psychosom Res* 2006; **61**: 349–358.
36 Weissman MM, Fyer AJ, Haghighi F, Heiman G, Deng Z, Hen R *et al*. Potential panic disorder syndrome: clinical and genetic linkage evidence. *Am J Med Genet* 2000; **96**: 24–35.
37 Badner JA, Gershon ES. Meta-analysis of whole-genome linkage scans of bipolar disorder and schizophrenia. *Mol Psychiatry* 2002; **7**: 405–411.
38 Potash JB, Zandi PP, Willour VL, Lan TH, Huo Y, Avramopoulos D *et al*. Suggestive linkage to chromosomal regions 13q31 and 22q12 in families with psychotic bipolar disorder. *Am J Psychiatry* 2003; **160**: 680–686.
39 McGuffin P, Knight J, Breen G, Brewster S, Boyd PR, Craddock N *et al*. Whole genome linkage scan of recurrent depressive disorder from the depression network study. *Hum Mol Genet* 2005; **14**: 3337–3345.
40 Sullivan GM, Coplan JD, Kent JM, Gorman JM. The noradrenergic system in pathological anxiety: a focus on panic with relevance to generalized anxiety and phobias. *Biol Psychiatry* 1999; **46**: 1205–1218.
41 Neumeister A, Daher RJ, Charney DS. Anxiety disorders: noradrenergic neurotransmission. *Handb Exp Pharmacol* 2005; **169**: 205–223.

Supplementary Information accompanies the paper on the Molecular Psychiatry website (http://www.nature.com/mp)

Dual involvement of G-substrate in motor learning revealed by gene deletion

Shogo Endo[a,1], Fumihiro Shutoh[b,1], Tung Le Dinh[c,1], Takehito Okamoto[b], Toshio Ikeda[d], Michiyuki Suzuki[e], Shigenori Kawahara[e], Dai Yanagihara[f], Yamato Sato[f], Kazuyuki Yamada[g], Toshiro Sakamoto[a], Yutaka Kirino[e], Nicholas A. Hartell[h], Kazuhiko Yamaguchi[c], Shigeyoshi Itohara[d], Angus C. Nairn[i], Paul Greengard[j], Soichi Nagao[b], and Masao Ito[c,2]

[a]Unit for Molecular Neurobiology of Learning and Memory, Okinawa Institute of Science and Technology, Uruma 904-2234, Japan; [b]Laboratory for Motor Learning Control, [c]Laboratory for Memory and Learning, [d]Laboratory for Behavioral Genetics, and [g]Support Unit for Animal Experiment, Research Resources Center, RIKEN Brain Science Institute, Wako 351-0198, Japan; [e]Laboratory for Neurobiophysics, School of Pharmaceutical Sciences, University of Tokyo, Tokyo 113-0033, Japan; [f]Department of Life Sciences, Graduate School of Arts and Sciences, University of Tokyo, Tokyo 153-8902, Japan; [h]Department of Cell Physiology and Pharmacology, University of Leicester, Leicester LE1 9HN, United Kingdom; [i]Department of Psychiatry, Yale University School of Medicine, New Haven, CT 06519; and [j]Laboratory for Molecular and Cellular Neuroscience, The Rockefeller University, New York, NY 10021-6399

Contributed by Masao Ito, December 30, 2008 (sent for review December 7, 2008)

In this study, we generated mice lacking the gene for G-substrate, a specific substrate for cGMP-dependent protein kinase uniquely located in cerebellar Purkinje cells, and explored their specific functional deficits. G-substrate–deficient Purkinje cells in slices obtained at postnatal weeks (PWs) 10–15 maintained electrophysiological properties essentially similar to those from WT littermates. Conjunction of parallel fiber stimulation and depolarizing pulses induced long-term depression (LTD) normally. At younger ages, however, LTD attenuated temporarily at PW6 and recovered thereafter. In parallel with LTD, short-term (1 h) adaptation of optokinetic eye movement response (OKR) temporarily diminished at PW6. Young adult G-substrate knockout mice tested at PW12 exhibited no significant differences from their WT littermates in terms of brain structure, general behavior, locomotor behavior on a rotor rod or treadmill, eyeblink conditioning, dynamic characteristics of OKR, or short-term OKR adaptation. One unique change detected was a modest but significant attenuation in the long-term (5 days) adaptation of OKR. The present results support the concept that LTD is causal to short-term adaptation and reveal the dual functional involvement of G-substrate in neuronal mechanisms of the cerebellum for both short-term and long-term adaptation.

cerebellum | long-term depression | optokinetic response | Purkinje cell

The G-substrate purified from rabbit cerebellum is one of the few preferred substrates for cGMP-dependent protein kinase (PKG) (1–8). It is positioned at the downstream end of the cascade linking nitric oxide (NO), soluble guanylate cyclase, cGMP, and PKG. The target(s) for NO is located within Purkinje cells (9–12), where diffusing NO activates soluble guanylate cyclase (13), which, in turn, enhances PKG activity (14). Immunohistochemical studies have revealed that G-substrate is uniquely concentrated in cerebellar Purkinje cells (2, 6, 7, 15, 16). In cerebellar slices, G-substrate in Purkinje cells is effectively phosphorylated in response to a membrane-permeable analogue of cGMP that activates PKG (9). Phosphorylated G-substrate acts as a potent inhibitor of protein phosphatase (PP) 1 and PP2A (6–8). We now have generated G-substrate knockout mice to investigate further the functional roles of G-substrate at cellular and behavioral levels.

Each component of the NO-cGMP-PKG pathway has so far been shown to be required for the induction of cerebellar long-term depression (LTD) (12, 17–24), a characteristic form of synaptic plasticity displayed by Purkinje cells (25). In LTD, synaptic transmission from parallel fibers (PFs) to Purkinje cells is persistently depressed after conjunctive stimulation of the PFs and climbing fibers (CFs). CF stimuli can be replaced by application of depolarizing pulses to the Purkinje cell membrane. Peculiarly, NO is not required for LTD induction in young cultured Purkinje cells (26), suggesting that the NO-cGMP-PKG pathway acts as a modulator whose requirement for LTD may depend on various circumstances (27).

LTD has been considered to provide a cellular mechanism of motor learning (25). Here, we report a distinctive age-dependent deficit of LTD induction in G-substrate–deficient Purkinje cells; LTD occurs at postnatal week (PW) 4 but diminishes at PW5–6 and then recovers at PW10 afterward. We also examined how the age-dependent diminution of LTD is reflected in the age profile of adaptation of optokinetic eye movement response (OKR), a simple form of motor learning. OKR adaptation is an increase of OKR gain induced by continuous oscillation of a screen around a stationary animal and is abolished by gene knockout (28) or pharmacological inhibition of neural NOS (28, 29). As very recently reported, OKR adaptation (30), as well as vestibulo-ocular reflex (VOR) adaptation (31), has 2 distinct phases underlain by different neural mechanisms. The short-term adaptation occurring during 1 h of training has its memory site in the cerebellar cortex of the flocculus, whereas the long-term adaptation accumulated during repeated 5-day training sessions is an event that takes place somewhere else, because the latter is maintained even after a glutamate antagonist (31) or lidocaine (30) has blocked cerebellar cortical activity. There is some evidence indicating that long-term OKR adaptation has its memory site in vestibular nuclear neurons (30).

In this study, we demonstrate in G-substrate knockout mice that the short-term OKR adaptation diminishes in an age-dependent manner in parallel with LTD amplitude reduction. G-substrate knockout affects the LTD induction and short-term OKR adaptation only temporarily around PW6; however, young adult mice at PW12 prove to be free of these deficits. We demonstrate that they are also free of deficits in other motor learning tasks, including eyeblink conditioning (32), motor coordination (33), and adaptive locomotion (34). Eventually, a significant depression of the long-term OKR adaptation is the only deficit exhibited by PW12 G-substrate knockout mice. Thus, the functional role of G-substrate gene is defined by its differential involvement in LTD-driven short-term OKR adaptation and otherwise initiated long-term OKR adaptation.

Author contributions: S.E., F.S., T.L.D., T.I., S.K., D.Y., Y.S., K. Yamada, Y.K., S.I., A.C.N., P.G., S.N., and M.I. designed research; S.E., F.S., T.L.D., T.O., T.I., M.S., S.K., D.Y., Y.S., K. Yamada, N.A.H., and K. Yamaguchi performed research; S.E., F.S., T.L.D., T.O., D.Y., Y.S., T.S., N.A.H., K. Yamaguchi, S.N., and M.I. analyzed data; and S.E. and M.I. wrote the paper.

The authors declare no conflict of interest.

Freely available online through the PNAS open access option.

[1]S.E., F.S., and T.L.D. contributed equally to this work.

[2]To whom correspondence should be addressed. E-mail: masao@brain.riken.jp.

This article contains supporting information online at www.pnas.org/cgi/content/full/0813341106/DCSupplemental.

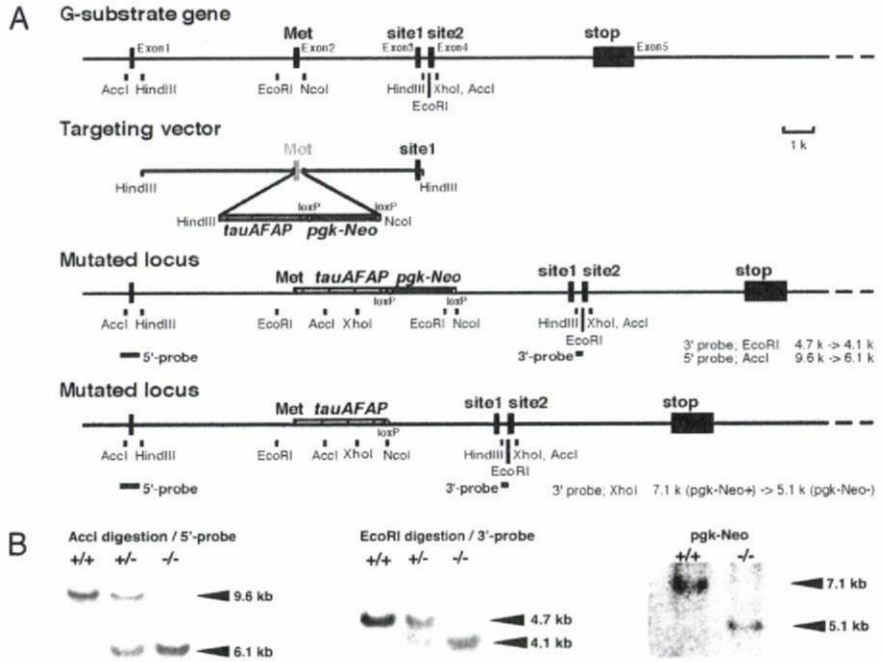

Fig. 1. Generation of G-substrate knockout mice. (*A*) Gene structure of mouse G-substrate and targeting vector for the generation of G-substrate knockout mice. (*B*) Confirmation of G-substrate knockout by Southern blot analysis. Restriction-enzyme–digested genomic DNA was subjected to Southern blot hybridization analysis. The band shift attributable to the homologous recombination was confirmed by probing the blot with ^{32}P-labeled 3′- and 5′-probes, as indicated in the figure. The removal of the selection marker, pgk-Neo cassette, was also confirmed by Southern blot analysis using the ^{32}P-labeled 3′-probe.

Results

Generation of G-Substrate Knockout Mice. The G-substrate gene consists of 5 exons and 4 introns (Fig. 1*A*). The initiation Met is in exon 2, and the 2 PKG phosphorylation sites are in separate exons (exons 3 and 4). For the generation of G-substrate knockout mice, the G-substrate gene was disrupted by insertion of DNA encoding a selection marker (pgk-neo cassette) and tau-AFAP in the first coding exon (exon 2) (Fig. 1*A*). Correct recombination was confirmed by Southern blot analysis of ES cells and F2 mice using 5′- and 3′-probes (Fig. 1*B*). The removal of the pgk-neo cassette, the selection marker in ES cells, was confirmed by Southern blot analysis (Fig. 1*B*). Homozygous mice deficient in G-substrate were obtained by mating heterozygous mice and had normal Mendelian distribution, showing lack of embryonic lethality. The homozygous G-substrate knockout mice appeared to develop and reproduce normally.

In samples from WT mice, mRNA was observed as a single band of 1.7 kb on Northern blot analysis; however, there was complete absence of G-substrate mRNA and immunoreactivity in the homozygous knockout mice [supporting information (SI) Fig. S1*A* and *B*]. Furthermore, no detectable G-substrate protein was observed in homogenates prepared from G-substrate knockout mice as demonstrated by immunoblotting of immunoprecipitates obtained using G-substrate antibody (Fig. S1*C*).

The results suggest that the homozygous G-substrate gene deletion led to a complete loss of the G-substrate mRNA and protein expression in the cerebellum. No major morphological changes were observed in the cerebellum or whole brain of homozygote mice as assessed by light microscopy (Fig. 2 *A* and *B*). The layer structures of the cerebellum were indistinguishable in WT and G-substrate knockout mice, as shown by Nissl staining of cerebellar slices. There were no apparent changes in the density, size, or shape of cerebellar Purkinje cells. In G-substrate knockout mice, the shape and path of Purkinje cells were easily visualized by fluorescence microscopy (Fig. 2*C*), given that AFAP, a GFP derivative, was expressed in G-substrate knockout mice under the control of the G-substrate promoter (Fig. 1). Primary and secondary dendrites and axon bundles were observed with bright fluorescence. Furthermore, axon bundles originating from Purkinje cells were clearly marked by AFAP. These axons course to the deep cerebellar nucleus and vestibular nucleus, as in normal mice.

Cerebellar LTD. In current clamp configuration with patch pipettes, we recorded from 120 Purkinje cells in acute slices from G-substrate knockout mice and from 118 Purkinje cells in acute slices from WT littermates. We confirmed that there were no statistically significant differences in membrane potential, membrane resistance, time course of PF-evoked excitatory postsynaptic potentials (EPSP), or waveform of complex spikes, except for a modest difference in paired-pulse facilitation of PF-EPSPs (Table S1). Stimulation of the white matter evoked full-sized CF responses in an all-or-none manner, and there was no evidence for multiple CF innervations of Purkinje cells.

Cerebellar LTD was induced by conjunction of PF stimulation with depolarizing pulses at 1 Hz for 5 min (see *Materials and Methods*). The induced LTD developed during the initial 20 min and was followed by a slow phase proceeding for another 40 min (Fig. 3*A*). Because our provisional tests showed variation in the expression of LTD in Purkinje cells deficient of G-substrate, we paid special attention to the possible age-dependent variation of LTD and examined mice at PW4 to PW15. As shown in Fig. 3*A*, WT Purkinje cells showed virtually identical average LTD time courses throughout life up to PW15. The magnitudes of LTD measured 41–50 min after the onset of 5 min of conjunction were about 20%, on average (Fig. 3*A*). In contrast, Purkinje cells lacking G-substrate showed virtually normal LTD at PW4, which then diminished to zero at PW6; thereafter it recovered to normal levels from PW10 onward (Fig. 3*B*). The histogram in Fig. 3*C* compares the LTD magnitude between G-substrate–deficient and WT Purkinje cells from PW4 to PW15. There was a significant difference in the LTD magnitude between the 2

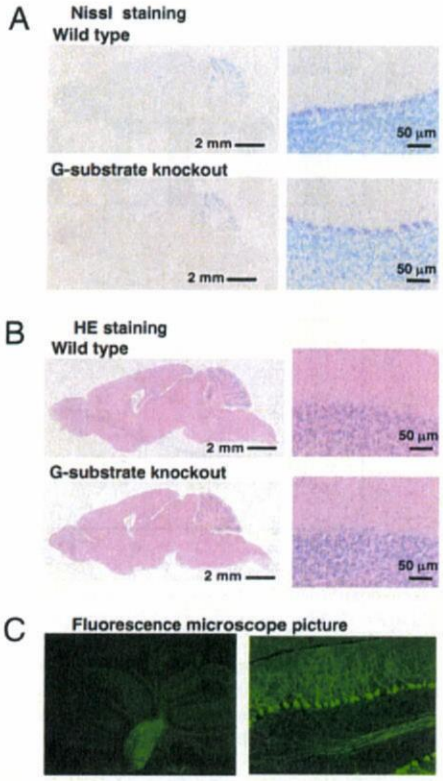

Fig. 2. Structures of cerebellum in WT and G-substrate knockout mice. (*A*) Nissl staining of cerebellar slices obtained from WT and G-substrate knockout mice. The thin sections (30 μm) were obtained from paraformaldehyde-fixed brain using a cryostat and were subjected to Nissl staining. (*B*) Hematoxylin and Eosin staining of brain slices obtained from WT and G-substrate knockout mice. (*C*) Fluorescence images of slices obtained from G-substrate knockout mice. The frozen thin sections (20 μm) were observed under a fluorescence microscope. AFAP, a GFP derivative, was expressed under the control of the G-substrate promoter.

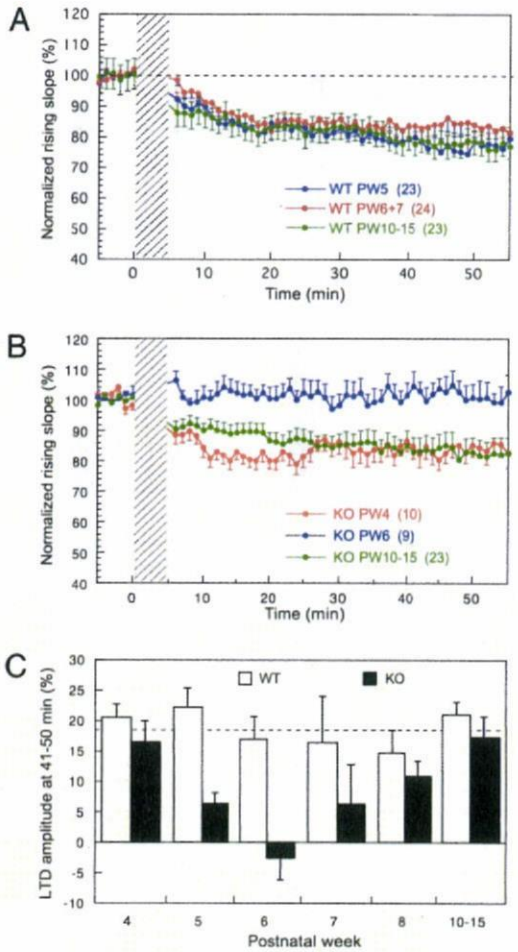

Fig. 3. Age-dependent expression of cerebellar LTD in G-substrate–lacking Purkinje cells. (*A*) Averaged time profile of 3 groups of WT Purkinje cells is shown with different colors. The ordinate illustrates the rising slope of PF-EPSPs relative to the average measured 5 min before conjunction, and the abscissa illustrates time. The oblique-shaded band indicates the application of conjunction of PF stimulation and depolarizing pulses. Number of Purkinje cells tested is shown in brackets. Vertical bars, SEs. (*B*) Similar to *A* but for G-substrate–deficient Purkinje cells. (*C*) Histograms showing LTD amplitude at 41–50 min for different PWs in WT and G-substrate–deficient Purkinje cells. Filled columns are G-substrate knockout mice, and empty columns are WT littermates. Vertical bars, SEs. The numbers of cells used for the experiments are as follows: for WT mice, PW4 (12), PW5 (23), PW6 (14), PW7 (10), PW8 (14), and PW10–15 (23); for G-substrate knockout mice, PW4 (10), PW5 (9), PW6 (9), PW7 (6), PW8 (11), and PW10–15 (29).

genotypes of Purkinje cells (2-way factorial ANOVA: $F_{1,\ 158} = 13.19$, $P = 0.004$). The LTD magnitude in G-substrate knockout mice showed a clear age-dependency (1-way ANOVA: $F_{5,\ 68} = 2.91$, $P = 0.019$), whereas the incidence and extent of LTD in WT mice did not ($F_{5,\ 90} = 0.671$, $P = 0.647$). The Dunnett post hoc test in Fig. 3*C* revealed that the LTD magnitude in G-substrate knockout Purkinje cells was significantly smaller than that in WT Purkinje cells at PW6 ($P < 0.01$) and PW5 ($P < 0.05$). LTD magnitudes in G-substrate knockout mice were also smaller at PW7 and PW8 (Fig. 3*C*), but these decreases were not statistically significant ($P > 0.05$).

Dynamics and Short-Term Adaptation of OKR. First, we examined the dynamic characteristics of the OKR (gain, phase, and screen frequency dependence) using sinusoidal screen oscillations (15° peak-to-peak, 0.11–0.33 Hz) in the light in 9 G-substrate knockout mice and 7 WT littermate mice at PW12 (Fig. S2). We observed no differences in the gains of OKR between G-substrate knockout and WT littermates (two-way repeated measures ANOVA: $F_{1,\ 14} = 0.082$, $P = 0.78$). Then, we examined the adaptation of OKR in 12 G-substrate knockout mice and 12 WT littermates at PW12. As shown in Fig. *4A*, no difference was observed in the "start gain" of OKR measured by sinusoidal screen oscillation (15° peak-to-peak, 0.17 Hz, maximum screen velocity of 7.9°/sec) between the 2 genotypes at PW12. These mice were subjected to 1-hr continuous screen oscillation with the same stimulus parameters to induce short-term OKR adaptation. The "end gain" of OKR was measured immediately after the 1-hr screen oscillation. The increase in the OKR gain during the 1-hr screen oscillation ([end gain] − [start gain]) represents the magnitude of the short-term OKR adaptation. As shown in Fig. *4B*, no significant difference was detected in short-term OKR adaptation in G-substrate knockout mice and WT littermates at PW12 [Student's *t* test: t (22) = 0.26, $P = 0.797$].

We also examined 14 G-substrate knockout mice and 10 WT mice at PW6 (all different from the mice examined previously at PW12). Fig *4C* shows that there was no significant difference in the start OKR gain between the 2 genotypes at PW6. However, a significant difference was detected in the short-term OKR adaptation between the 2 genotypes at PW6 (Fig. 4*D*); the magnitude of short-term OKR adaptation was smaller in G-substrate knockout mice than in WT mice [Student's *t* test: t (22) = 2.094, $P = 0.048$]. Furthermore, examination of the mice at PW4 and PW5 revealed a low OKR gain and poor short-term OKR adaptation for both G-substrate knockout and WT litter-

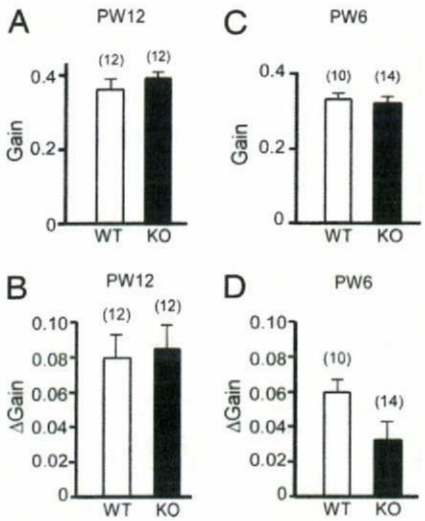

Fig. 4. OKR gain and short-term OKR adaptation. Mice were subjected to sinusoidal screen oscillation by 15° (peak-to-peak) at 0.17 Hz (maximum velocity, 7.9°/sec) in the light for 1 hr. (*A*) Start OKR gain before 1-hr screen oscillation at PW12. (*B*) OKR gain change obtained during 1-hr sustained screen oscillation at PW12. (*C*) Similar to *A* but at PW6. (*D*) Similar to *B* but at PW6. Filled columns represent G-substrate knockout (KO) mice, and empty columns represent WT mice. Vertical bars, SEs. The number of mice used is shown in brackets.

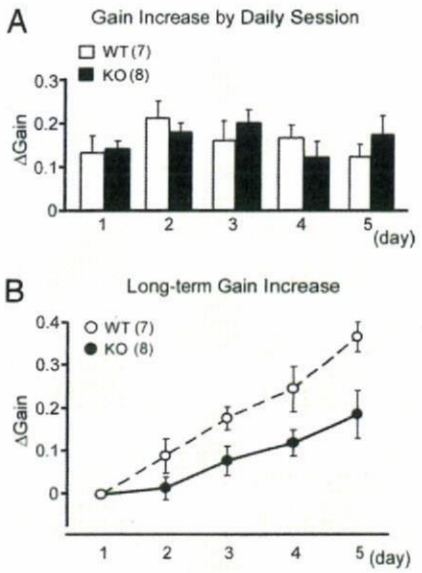

Fig. 5. Long-term adaptation of OKR. WT (n = 7) and G-substrate knockout (KO) mice (n = 8) at PW12–15 were exposed to 1-hr sustained screen oscillation every day for 5 days. The mice were kept in the dark, except during the screen oscillation. (*A*) Daily OKR adaptation. The ordinate illustrates ΔGain, gain changes obtained after 1-hr oscillation on each day. Filled columns are G-substrate KO mice, and empty columns are WT littermates. (*B*) Cumulative OKR gain changes induced through 5-day sessions. The ordinate illustrates ΔGain, increases of the start gains on each day as measured from the start gain at day 1. Hollow circles represent WT mice, and solid circles represent G-substrate KO mice.

mates (data not shown). It appears that the OKR neuronal circuit is immature at PW4 and PW5, such that short-term OKR adaptation occurs only rudimentarily. The results in Fig. 4 *B* and *D* suggest that the OKR neuronal circuit has matured considerably by PW6, although it might not be as complete as that at PW12, and that it expresses a deficit caused by G-substrate knockout. These interpretations are consistent with the results shown in Fig. 3*C* (i.e., LTD attenuates at PW6 but recovers at PW12).

Long-Term OKR Adaptation. Next, we examined long-term OKR adaptation by carrying out 1 session of 1-hr screen oscillation per day for 5 successive days. Fig. 5*A* shows that the daily gain changes ([end gain] − [start gain]) did not show significant differences between the WT and G-substrate knockout mice throughout 5 days (two-way repeated measures ANOVA: $F_{1,13} = 0.019, P = 0.893$). The increase in the daily gain recovered within 24 hr; however, the start gain before the 1-hr oscillation gradually increased at days 2–5 compared with the start gain at day 1, which we call long-term adaptation (30). Fig. 5*B* compares the gain increase induced by long-term OKR adaptation between the 2 genotypes. The gain increase of the G-substrate knockout mice was smaller than that of the WT mice throughout the 5-day session (two-way repeated measures ANOVA: $F_{1,13} = 6.508, P = 0.024$) (Fig. 5*B*). At the end of day 5, the start gain increased by 0.19 in G-substrate knockout mice, whereas it increased by 0.37 in the WT mice (Fig. 5*B*). Thus, G-substrate knockout mice are characterized by a partial but significant decrease in the rate of long-term OKR adaptation. The long-term OKR adaptation is not an accumulation of residuals of short-term adaptation, because the former remained intact with local application of lidocaine to the flocculus (30), which blocks the latter. The present results showing that, at PW12, long-term OKR adaptation attenuates, whereas short-term OKR adaptation occurs normally provide another line of evidence that the 2 types of OKR adaptation are underlain by different neural mechanisms.

General Behavior. Behavioral tests described in this article were carried out on young adult mice at PW12, unless otherwise stated. The overall behavioral properties of G-substrate knockout mice were not different from those of WT mice (summarized in Table S2). G-substrate knockout mice exhibited some decrease in locomotor activity in the open-field test; however, the data did not reach statistical significance, except for the distance moved in the dark condition (Fig. S3). The decreased distance moved in the open field might imply an emotional change in G-substrate knockout mice. However, we confirmed that G-substrate knockout mice have normal sensory systems, and they behaved normally in a variety of other emotional tests carried out in the entire test battery (Table S2). A further detailed analysis is required to identify the possible emotional change implied by the open-field test results.

Rotor Rod Test and Gait Analyses. Motor coordination was examined in the G-substrate knockout and WT mice using the rotor rod test at a speed of 8 rotations per min (rpm) (Fig. S4*A*) and 12 rpm (data not shown). G-substrate knockout mice and WT mice indistinguishably improved their retention time before falling during repeated trials (two-way repeated measures ANOVA: $F_{1,9} = 0.015$, $P = 0.907$). Furthermore, the results obtained 24 hr after the initial 10 trials at 8 rpm were not different between WT and G-substrate knockout mice (data not shown).

We examined the kinematics of gait using high-speed video recordings during treadmill locomotion to characterize locomotor movements. No significant differences were observed between WT and G-substrate knockout mice in terms of temporal parameters such as step cycle duration, swing phase duration, stance phase duration, and bisupport phase duration (Table S3). As the treadmill speed increased, the step cycle duration and stance phase duration decreased, although the swing phase duration remained nearly constant in both lines of mice. The angular excursions of the knee and ankle were similar in the WT and knockout mice, although the joints stayed in slightly ex-

tended positions in G-substrate knockout mice (Fig. S4 *B* and *C*). G-substrate knockout mice did not show any appreciable abnormality in motor coordination and hind limb kinematics during treadmill locomotion, and it is concluded that the gait in G-substrate knockout mice is not ataxic.

Eyeblink Conditioning. This is a well-established form of cerebellum-dependent motor learning (35), and some genetically modified mouse lines with impaired cerebellar LTD have been reported to show abnormality in eyeblink conditioning (36–40). In this study, G-substrate knockout mice acquired the task as quickly as the WT mice in delay eyeblink conditioning tasks (Fig. S5*A*) and in trace eyeblink conditioning tasks (Fig. S5*B*).

Discussion

Homozygotic G-substrate–deficient mice survived and were normal in terms of morphology of the cerebellum (Fig. 2) and other brain areas, general behaviors (Table S1 and Figs. S2 and S3), and reproduction. G-substrate knockout mice thus share a disturbance-free phenotype with Purkinje cell-specific (PKGI) knockout mice (24). This is partly because both PKG and G-substrate are localized in Purkinje cells, but it is also because the deletion of PKGI (24) or G-substrate (see *Results*) does not cause multiple innervations of Purkinje cells by CFs, which may lead to ataxia or seizure.

The temporary hiatus of LTD and short-term OKR adaptation in G-substrate knockout mice around PW6 may suggest that the NO-cGMP-PKG-G-substrate pathway becomes essential during this crucial stage of development. At other times, it plays an accessory role rather than an essential role. At the end of this pathway, PKG-phosphorylated G-substrate acts as a potent inhibitor of PP1 and PP2A (6–8). Complex involvement of PPs in cerebellar LTD has been observed in cultured Purkinje cells: myosin/moesin phosphatase (containing PP1 catalytic subunit in its complex) plays a major role at 9–16 days in vitro (DIV) (41), but at 22–35 DIV, PP2A takes over (42). Hence, it is possible that, underlying the age profile of LTD (Fig. 3*C*), G-substrate comes into play as a preferential inhibitor of PP2A with a delay of 6 weeks, and then is probably replaced by PW10 with another PP inhibitor, which is currently unknown. The results indicating that G-substrate knockout attenuates both cerebellar LTD and short-term OKR adaptation temporarily at the early stage of development (Figs. 3*C* and 4*D*) conform to previous results showing that blockade of LTD leads to impairment of short-term OKR adaptation (28). Together, these results consistently support the current view that LTD is an essential mechanism of cerebellum-dependent learning. In this context, a close association was also reported very recently in mice lacking delphilin in Purkinje cells, whose LTD induction and OKR adaptation were both enhanced (43). Temporary diminution of LTD, which is now shown to be associated with attenuation of short-term OKR adaptation in G-substrate knockout mice, may also impair other forms of motor learning such as motor coordination on the rotor rod and eyeblink conditioning. We leave analyses of this association to future study until the dual-phase mechanism, which is the basis of the present analysis of OKR adaptation, is also defined for other forms of motor learning.

In G-substrate knockout mice at PW12, LTD induction and short-term OKR adaptation occurred normally (Figs. 3*A* and 4*B*) but long-term adaptation was significantly impaired (Fig. 5*B*). This long-term adaptation is caused by a slowly developed potentiation of synaptic transmission or an intrinsic excitability in vestibular relay neurons (30). The partial impairment of long-term VOR adaptation was also reported to occur in Purkinje cell-specific PKGI-deficient mice with normal short-term adaptation (24). Therefore, the NO-cGMP-PKG-G-substrate cascade appears to play an essential role in the induction of long-term VOR and OKR adaptations, which cannot be compensated for by another pathway. Long-term VOR and OKR adaptations would share a common synaptic mechanism at vestibular relay neurons (44). How the lack of G-substrate in Purkinje cells impairs the adaptive mechanism in vestibular relay neurons is presently unknown. Preliminary results suggest that G-substrate undergoes intracellular translocation from the cell nucleus to cytosol in response to the membrane-permeable analogue of cGMP, 8-bromoguanosine 3′: 5′-cyclic monophosphate (M.S. and S.E., unpublished observation). Recently, the DARPP-32, a PP inhibitor in striatal neurons, was reported to translocate to the cell nuclei, and the translocation was associated with increased histone H3 phosphorylation, an important component of nucleosomal response such as transcription (45). G-substrate translocation may lead to changes in the state of protein phosphorylation in the nucleus and cytosol, or it may affect transcription-translation systems. These effects potentially affect molecular events in the axon terminals of Purkinje cells, which would, in turn, act on vestibular relay neurons transsynaptically.

Conclusion

We have shown that G-substrate knockout causes dual deficits in motor learning. It attenuates cerebellar LTD and associated short-term adaptation temporarily at the early stage of development, consistent with the current view that LTD is an essential mechanism of cerebellum-dependent learning, and it also persistently impairs long-term adaptation of OKR. Otherwise, the G-substrate knockout mice are surprisingly free of disturbances in neuronal functions or behaviors. These mice provide a good model for the investigation of cellular, molecular, and genetic mechanisms underlying the short-term and long-term adaptations of motor behaviors.

Materials and Methods

Isolation and Targeted Disruption of Mouse G-Substrate Gene. The cDNA for mouse G-substrate was obtained from mouse cerebellum by PCR using the primer sets based on human (6) and rat (7) G-substrate cDNA. Then, a mouse C57BL/6 genomic library (46) constructed in a BAC plasmid was screened using a random-primed cDNA probe for mouse G-substrate. Positive clones were analyzed by restriction mapping and sequencing using a GPS system (NEB).

The standard technique for gene targeting (47) was used. Targeting vectors were constructed in pBluescript to replace exon 2 of the G-substrate gene, which encodes the initiation site Met, with the tau-AFAP-pgk-Neo cassette (Fig. 1). Detailed methods for confirmation of positive clones and generation of chimeric mice and mice harboring the knockout allele are provided in *SI Text* and in Fig. 1. Total RNA was isolated from the cerebellum using Sepasol (Nakalai Tesque) and was analyzed by Northern blotting analysis using a ^{32}P-labeled mouse G-substrate probe (corresponding to nucleotides 129–608 of AF071562). The blots were hybridized in QuikHyb hybridization solution (Stratagene) at 65 °C overnight and washed with 0.2× SSC containing 0.1% SDS. The hybridization signals on the blots were analyzed using a phosphorimager BAS5000 (Fuji Film).

Immunohistochemistry. Paraformaldehyde-fixed brain slices were stained with affinity-purified anti-G-substrate antibodies (7). Immunoreaction was visualized with Alexa Fluor 546-conjugated anti-mouse IgG (Molecular Probes). Fluorescent image stainings were obtained using an FX1000 confocal fluorescence microscope (Olympus).

Immunoprecipitation and Immunoblots. Mouse cerebella were homogenized in extraction buffer containing 50 mM Tris-HCl (pH 7.5), protease inhibitor mixture (Roche Diagnostics), 25 mM β-glycerophosphate, and 1% Nonidet P-40. The homogenates were centrifuged at 100,000 × *g* for 1 h, and the resulting supernatants were then subjected to immunoprecipitation. Affinity-purified rabbit anti-G-substrate antibodies against the amino terminus portion or the carboxyl terminus portion of G-substrate were used for the immunoprecipitation (7). Immunoprecipitates were subjected to SDS/PAGE, followed by immunoblot analysis. The protein concentration was determined by the method of Bradford (48) using BSA as the standard.

Slice Experiments. Under general anesthesia by ether inhalation, mice were decapitated and the cerebellum was excised. Sagittal slices of 300 μm thickness were prepared from the vermis. The recording chamber was perfused with oxygenated Ringer's solution containing 100 μM picrotoxin at 30–31 °C. Under an upright microscope, whole-cell patch-clamp recordings were performed using borosilicate pipettes (resistance, 3–5 MΩ). A Multiclamp700A amplifier (Axon) and pClamp 9 software (Axon) were used. PFs were focally stimulated through a glass pipette. To induce LTD, depolarizing pulses of 200 msec duration were applied to Purkinje cell membrane and adjusted (within 2 nA) to evoke at least 1 Ca^{2+} spike. PFs were stimulated with double pulses (each 0.1 msec in duration) paired at 50-msec intervals timed in such a way that the first pulse fell 30 msec later than the onset of each depolarizing pulse. The combination of double PF stimuli and a depolarizing pulse was repeated at 1 Hz for 5 min (300 pulses) in each trial of LTD induction.

Behavioral Analysis. For this purpose, mice were backcrossed with C57BL/6 for at least 5 generations. Protocols for all animal experiments were approved by the animal experiment committees of the RIKEN Brain Science Institute, Okinawa Institute of Science and Technology, and the other authors' institutions. Maximum efforts were made to reduce the stress of the mice. Detailed methods for the behavioral analyses, including general behaviors, eye movement, eyeblink conditioning, and rotor rod and treadmill locomotion, are provided in *SI Text*.

ACKNOWLEDGMENTS. We thank Ms. Masako Suzuki for the generation of G-substrate knockout mice and Dr. Mariko Sumi and Ms. Yumiko Motoyama for other technical assistance. MS12 cells were a generous gift from the Meiji Dairies Corporation. This work was supported by a grant for collaboration of the Okinawa Institute of Science and Technology and RIKEN Brain Science Institute and by grants from Ministry of Education, Culture, Sports, Science, and Technology of Japan.

1. Schlichter DJ, Casnellie JE, Greengard P (1978) An endogenous substrate for cGMP-dependent protein kinase in mammalian cerebellum. *Nature* 273:61–62.
2. Schlichter DJ, *et al.* (1980) Localization of cyclic GMP-dependent protein kinase and substrate in mammalian cerebellum. *Proc Natl Acad Sci USA* 77:5537–5541.
3. Aswad DW, Greengard P (1981) A specific substrate from rabbit cerebellum for guanosine 3′:5′-monophosphate-dependent protein kinase. I. Purification and characterization. *J Biol Chem* 256:3487–3493.
4. Aswad DW, Greengard P (1981) A specific substrate from rabbit cerebellum for guanosine 3′:5′-monophosphate-dependent protein kinase. II. Kinetic studies on its phosphorylation by guanosine 3′:5′-monophosphate-dependent and adenosine 3′:5′-monophosphate-dependent protein kinases. *J Biol Chem* 256:3494–3500.
5. Aitken A, *et al.* (1981) A specific substrate from rabbit cerebellum for guanosine-3′:5′-monophosphate-dependent protein kinase. III. Amino acid sequences at the two phosphorylation sites. *J Biol Chem* 256:3501–3506.
6. Endo S, *et al.* (1999) Molecular identification of human G-substrate, a possible downstream component of the cGMP-dependent protein kinase cascade in cerebellar Purkinje cells. *Proc Natl Acad Sci USA* 96:2467–2472.
7. Endo S, Nairn AC, Greengard P, Ito M (2003) Thr123 of rat G-substrate contributes to its action as a protein phosphatase inhibitor. *Neurosci Res (NY)* 45:79–89.
8. Hall KU, *et al.* (1999) Phosphorylation-dependent inhibition of protein phosphatase-1 by G-substrate. A Purkinje cell substrate of the cyclic GMP-dependent protein kinase. *J Biol Chem* 274:3485–3495.
9. Hartell NA (1994) cGMP acts within cerebellar Purkinje cells to produce long term depression via mechanisms involving PKC and PKG. *NeuroReport* 5:833–836.
10. Lev-Ram V, *et al.* (1995) Long-term depression in cerebellar Purkinje neurons results from coincidence of nitric oxide and depolarization-induced Ca^{2+} transients. *Neuron* 15:407–415.
11. Lev-Ram V, *et al.* (1997) Synergies and coincidence requirements between NO, cGMP, and Ca^{2+} in the induction of cerebellar long-term depression. *Neuron* 18:1025–1038.
12. Shin JH, Linden DJ (2005) An NMDA receptor/nitric oxide cascade is involved in cerebellar LTD but is not localized to the parallel fiber terminal. *J Neurophysiol* 94:4281–4289.
13. Stone JR, Marlette MA (1996) Soluble guanylate cyclase from bovine lung: Activation with nitric oxide and carbon monoxide and spectral characterization of the ferrous and ferric states. *Biochemistry* 35:1094–1099.
14. Hartell NA, Furuya S, Jacoby S, Okada D (2001) Intercellular action of nitric oxide increases cGMP in cerebellar Purkinje cells. *NeuroReport* 12:25–28.
15. Detre JA, Nairn AC, Aswad DW, Greengard P (1984) Localization in mammalian brain of G-substrate, a specific substrate for guanosine 3′, 5′-cyclic monophosphate-dependent protein kinase. *J Neurosci* 4:2843–2849.
16. Qian Y, *et al.* (1996) cGMP-dependent protein kinase in dorsal root ganglion: Relationship with nitric oxide synthase and nociceptive neurons. *J Neurosci* 16:3130–3138.
17. Crepel F, Jaillard D (1990) Protein kinases, nitric oxide and long-term depression of synapses in the cerebellum. *NeuroReport* 1:122–136.
18. Ito M, Karachot L (1990) Messengers mediating long-term desensitization in cerebellar Purkinje cells. *NeuroReport* 1:129–132.
19. Shibuki K, Okada D (1991) Endogenous nitric oxide release required for long-term synaptic depression in the cerebellum. *Nature* 349:326–328.
20. Daniel H, Hemart N, Jaillard D, Crepel F (1993) Long-term depression requires nitric oxide and guanosine 3′:5′ cyclic monophosphate production in rat cerebellar Purkinje cells. *Eur J Neurosci* 5:1079–1082.
21. Lev-Ram V, *et al.* (1997) Absence of cerebellar long-term depression in mice lacking neuronal nitric oxide synthase. *Learn Mem* 4:169–717.
22. Boxall AR, Garthwaite J (1996) Long-term depression in rat cerebellum requires both NO synthase and NO-sensitive guanylyl cyclase. *Eur J Neurosci* 8:2209–2212.
23. Jacoby S, Sims RE, Hartell NA (2001) Nitric oxide is required for the induction and heterosynaptic spread of cerebellar LTP. *J Physiol (London)* 535:825–839.
24. Feil R, *et al.* (2003) Impairment of LTD and cerebellar learning by Purkinje cell-specific ablation of cGMP-dependent protein kinase I. *J Cell Biol* 163:295–302.
25. Ito M (2001) Cerebellar long-term depression: Characterization, signal transduction, and functional roles. *Physiol Rev* 81:1143–1195.
26. Linden DJ, Connor JA (1992) Long-term depression of glutamate currents in cultured cerebellar Purkinje neurons does not require nitric oxide signaling. *Eur J Neurosci* 4:10–15.
27. Ito M (2002) The molecular organization of cerebellar long-term depression. *Nat Rev Neurosci* 3:896–902.
28. Katoh A, Kitazawa H, Itohara S, Nagao S (2000) Inhibition of nitric oxide synthesis and gene knockout of neuronal nitric oxide synthase impaired adaptation of mouse optokinetic response eye movement. *Learn Mem* 7:220–226.
29. Nagao S, Ito M (1991) Subdural application of hemoglobin to the cerebellum blocks vestibuloocular reflex adaptation. *NeuroReport* 2:193–196.
30. Shutoh F, *et al.* (2006) Memory trace of motor learning shifts transsynaptically from cerebellar cortex to nuclei for consolidation. *Neuroscience* 139:767–777.
31. Kassardjian CD, *et al.* (2005) The site of a motor memory shifts with consolidation. *J Neurosci* 25:7979–7985.
32. Chapman PF, Atkins CM, Allen MT, Haley JE, Steinmetz JE (1992) Inhibition of nitric oxide synthesis impairs two different forms of learning. *NeuroReport* 3:567–570.
33. Kriegsfeld LJ, *et al.* (1991) Nocturnal motor coordination deficits in neuronal nitric oxide synthase knock-out mice. *Neuroscience* 89:311–315.
34. Yanagihara D, Kondo I (1996) Nitric oxide plays a key role in adaptive control of locomotion in cat. *Proc Natl Acad Sci USA* 93:13292–13297.
35. Kim JJ, Thompson RF (1997) Cerebellar circuits and synaptic mechanisms involved in classical eyeblink conditioning. *Trends Neurosci* 20:177–181.
36. Aiba A, *et al.* (1994) Deficient cerebellar long-term depression and impaired motor learning in mGluR1 mutant mice. *Cell* 79:377–388.
37. Kishimoto Y, *et al.* (2001) Impaired delay but normal trace eyeblink conditioning in PLCβ4 mutant mice. *NeuroReport* 12:2919–2922.
38. Kishimoto Y, *et al.* (2001) Classical eyeblink conditioning in glutamate receptor subunit δ2 mutant mice is impaired in the delay paradigm but not in the trace paradigm. *Eur J Neurosci* 13:1249–1253.
39. Kishimoto Y, *et al.* (2002) mGluR1 in cerebellar Purkinje cells is required for normal association of temporally contiguous stimuli in classical conditioning. *Eur J Neurosci* 16:2416–2424.
40. Shibuki K, *et al.* (1996) Deficient cerebellar long-term depression, impaired eyeblink conditioning, and normal motor coordination in GFAP mutant mice. *Neuron* 16:587–599.
41. Eto M, Bock R, Brautigan DL, Linden DJ (2002) Cerebellar long-term synaptic depression requires PKC-mediated activation of CPI-17, a myosin/moesin phosphatase inhibitor. *Neuron* 36:1145–1158.
42. Launey T, *et al.* (2004) Protein phosphatase 2A inhibition induces cerebellar long-term depression and declustering of synaptic AMPA receptor. *Proc Natl Acad Sci USA* 101:6766–6781.
43. Takeuchi T, *et al.* (2008) Enhancement of both long-term depression induction and optokinetic response adaptation in mice lacking delphilin. *PloS ONE* 3:e2297.
44. Ito M (2006) Cerebellar circuitry as a neuronal machine. *Prog Neurobiol* 78:272–303.
45. Stipanovich A, *et al.* (2008) A phosphatase cascade by which rewarding stimuli control nucleosomal response. *Nature* 453:879–884.
46. Osoegawa K, *et al.* (2000) Bacterial artificial chromosome libraries for mouse sequencing and functional analysis. *Genome Res* 10:116–128.
47. Gomi H, *et al.* (1995) Mice devoid of the glial fibrillary acidic protein develop normally and are susceptible to scrapie prions. *Neuron* 14:29–41.
48. Bradford MM (1976) A rapid and sensitive method for the quantitation of microgram quantities of protein utilizing the principle of protein-dye binding. *Anal Biochem* 72:248–254.

Developmental Cell
Article

Committed Neuronal Precursors Confer Astrocytic Potential on Residual Neural Precursor Cells

Masakazu Namihira,[1,5] Jun Kohyama,[1] Katsunori Semi,[1] Tsukasa Sanosaka,[1] Benjamin Deneen,[2] Tetsuya Taga,[3,4] and Kinichi Nakashima[1,*]
[1]Laboratory of Molecular Neuroscience, Graduate School of Biological Sciences, Nara Institute of Science and Technology, 8916-5 Takayama, Ikoma, Nara 630-0101, Japan
[2]Division of Biology 216-76, California Institute of Technology, Pasadena, CA 91125, USA
[3]Division of Cell Fate Modulation, Institute of Molecular Embryology and Genetics, Kumamoto University, 2-2-1 Honjo, Kumamoto 860-0811, Japan
[4]Department of Stem Cell Regulation, Medical Research Institute, Tokyo Medical and Dental University, 1-5-45, Yushima, Bunkyo-ku, Tokyo, 113-8510, Japan
[5]Present address: Department of Human Genetics, David Geffen School of Medicine, University of California at Los Angeles, Los Angeles, CA 90095, USA
*Correspondence: kin@bs.naist.jp
DOI 10.1016/j.devcel.2008.12.014

SUMMARY

During midgestation, mammalian neural precursor cells (NPCs) differentiate only into neurons. Generation of astrocytes is prevented at this stage, because astrocyte-specific gene promoters are methylated. How the subsequent switch from suppression to expression of astrocytic genes occurs is unknown. We show in this study that Notch ligands are expressed on committed neuronal precursors and young neurons in mid-gestational telencephalon, and that neighboring Notch-activated NPCs acquire the potential to become astrocytes. Activation of the Notch signaling pathway in midgestational NPCs induces expression of the transcription factor nuclear factor I, which binds to astrocytic gene promoters, resulting in demethylation of astrocyte-specific genes. These findings provide a mechanistic explanation for why neurons come first: committed neuronal precursors and young neurons potentiate remaining NPCs to differentiate into the next cell lineage, astrocytes.

INTRODUCTION

Fetal telencephalic neuroepithelial cell populations in mammalian embryonic brain contain multipotent neural precursor cells (NPCs) that can self-renew and give rise to the three major central nervous system (CNS) cell types—neurons, astrocytes, and oligodendrocytes. However, NPCs do not express multipotentiality in early gestation, differentiating only into neurons at midgestation; they gradually begin to display multipotentiality, and differentiate into astrocytes and oligodendrocytes during late gestation (Temple, 2001). The mechanisms driving this stepwise process in the developing brain are poorly understood, although cytokine-induced activation of the janus kinase (JAK)-signal transducer and activator of transcription (STAT) pathway, and changes in DNA methylation of astrocyte-specific gene promoters, are thought to be intimately involved in the regulation of astrogliogenesis (Fan et al., 2005; He et al., 2005; Takizawa et al., 2001).

Since neurons are produced before NPCs gain the potential to differentiate into astrocytes, pregenerated neurons are strong candidates to confer astrogliogenic potential on NPCs. In this context, it has been suggested that neuron-secreted cardiotrophin (CT)-1, a member of the interleukin (IL)-6 cytokine family that activates the gp130-JAK-STAT pathway, induces astrocytic differentiation of mouse NPCs at embryonic day (E) 13.5 (Barnabe-Heider et al., 2005). These findings do not, however, exclude the possibility that, prior to E13.5, cortical precursors undergo an intrinsic change, such as demethylation of astrocytic gene promoters (Takizawa et al., 2001), that allows them to respond to cytokines.

Notch receptors and their ligands, molecules best known for influencing cell fate decisions through direct cell-cell contact (Louvi and Artavanis-Tsakonas, 2006; Nye and Kopan, 1995; Weinmaster, 1997), participate in a wide variety of biological events, including fate decision of NPCs. Upon ligand binding, the intracellular domain of Notch (NICD) is released from the plasma membrane and translocates into the nucleus, where it converts the CBF1(RBP-J)/Su(H)/LAG1 (CSL) repressor complex into an activator complex. The NICD/CSL1 activator complex targets genes such as *Hes* and *Hesr* (Hes-related protein), which encode basic helix-loop-helix transcriptional regulators that antagonize proneural genes, and thus neurogenesis (Bertrand et al., 2002; Kato et al., 1997). However, it is largely unknown how the Notch signaling pathway is involved in neurogenic-to-gliogenic switching during CNS development.

Recently, it has been reported that nuclear factor I (NFI) A, a member of a family of CCAAT box element-binding transcription factors (Gronostajski, 2000), is both necessary and sufficient to promote glial fate specification in embryonic spinal cord progenitors in vivo (Deneen et al., 2006). Previous studies had shown that adult mice deficient for NFIA or NFIB exhibited

a reduction in cortical glial fibrillary acidic protein (GFAP), a typical marker protein for astrocytes (das Neves et al., 1999; Steele-Perkins et al., 2005), as well as a reduction in the number of midline glia (Shu et al., 2003). It was further shown that E18.5 embryos lacking either NFIA or NFIB displayed a reduction in spinal cord GFAP expression (Deneen et al., 2006), and that misexpression of NFIA or NFIB was sufficient to accelerate GFAP expression in astrocytic precursors by several days in vivo and in vitro. These data indicate that NFIA/B promote the terminal differentiation of astrocytes. Furthermore, *gfap* expression is likely to be directly regulated by NFIA/B, as functional NFI-binding sites have been identified in the promoter (Cebolla and Vallejo, 2006). However, the precise relationships between NFIs and other factors, such as the JAK-STAT and Notch signaling pathways and DNA methylation, in the regulation of astrocyte differentiation of NPCs have not been elucidated.

Many studies have provided us with an integrated view of the gliogenic switch, with multiple extrinsic and intrinsic mechanisms acting in concert to induce gliogenesis when an appropriate number of neurons has been generated. Nevertheless, how promoter methylation changes are induced, and why neurons have to be produced first from NPCs during brain development, remain outstanding questions. In this study, we provide an explanation for the sequential differentiation of NPCs into neurons and then astrocytes through the epigenetic modification during embryonic brain development.

RESULTS

Neurons Confer Astrocyte Differentiation Potential on NPCs via Notch Signal Activation

It has been suggested that neuron-secreted CT-1 induces astrocytic differentiation of mouse NPCs at E13.5. However, CT-1 and leukemia inhibitory factor (LIF), which activates the same signaling pathway as CT-1, failed to do so at an earlier stage (E11.5), and did not evoke demethylation of the astrocyte-specific *gfap* gene promoter (Figures 1A and 1D and data not shown). We therefore sought to examine the involvement of cell-to-cell interactions, in addition to that of secreted factors. As a first step, we cocultured E11.5 NPCs with embryonic cortical neurons, and found that they could differentiate into GFAP-positive astrocytes in the presence of LIF (Figures 1B, 1B′, and 1D). Notch signaling is one of the most important mediators of intercellular interaction during CNS development (Louvi and Artavanis-Tsakonas, 2006). Several recent studies have suggested that Notch1 is activated in proliferating NSCs (Tokunaga et al., 2004; Androutsellis-Theotokis et al., 2006; Yoshimatsu et al., 2006), and may play a decisive role in promoting glial development (Grandbarbe et al., 2003). When we performed the same coculture experiment as above, but with a γ-secretase inhibitor (N-[N-(3,5-Difluorophenacetyl-L-Alanyl)]-S-phenylglycine t-butyl ester) to inhibit cleavage of NICD, which is indispensable for Notch signal activation (Androutsellis-Theotokis et al., 2006), astrocytic differentiation was abolished (Figures 1C, 1C′, and 1D). Moreover, ectopic expression of the intracellular-acting Notch signal inhibitor *Dll3* (Ladi et al., 2005) in E11.5 NPCs also resulted in the inhibition of astrocytic differentiation in coculture conditions (see Figure S1 available online). Using the TP1-Venus Notch-activation reporter plasmid (Kohyama et al., 2005), we further confirmed that Notch signaling was indeed activated in NPCs located in close contact with embryonic cortical neurons (Figure S2). These data implicated Notch signaling in the embryonic neuron-induced potentiation of NPCs to differentiate into astrocytes.

Activation of Notch Signal Is Sufficient for Acquisition of Astrocyte Differentiation in NPCs

Next, we sought to determine whether Notch activation is sufficient for astrocytic differentiation of midgestational NPCs. E11.5 NPCs were infected with retroviruses engineered to express either green fluorescent protein (GFP) alone or GFP together with NICD (Takizawa et al., 2003). The following day, LIF was added to the culture, and the cells were incubated for an additional 3 days. In contrast to NPCs infected with control virus, a dramatic induction of GFAP-positive astrocytic differentiation was observed in NICD-expressing NPCs after LIF stimulation (Figures 1F–1G), indicating that the activation of Notch signaling enabled precocious astrocytic differentiation of midgestational NPCs that would otherwise differentiate only into neurons. In the absence of LIF, no GFAP-positive cells were observed in control or NICD-expressing NPCs (data not shown). Thus, although these experiments demonstrated that Notch activation confers astrogliogenic potential on midgestational NPCs, LIF stimulation was still required to induce differentiation of NPCs into GFAP-positive astrocytes.

Since an inverse correlation exists between the potential of NPCs to express *gfap* and the methylation status of the STAT3-binding site within the *gfap* promoter (Fan et al., 2005; Takizawa et al., 2001), we wished to determine whether NICD expression induces demethylation of this site. Four days after virus infection, GFP-positive cells were sorted by fluorescence-activated cell sorting (FACS) and their genomic DNA was subjected to bisulfite sequencing. In freshly prepared E11.5 NPCs, the STAT3 binding site was highly methylated (Figures 1H and 1I), as has been shown previously (Takizawa et al., 2001). The STAT3 site became slightly and spontaneously demethylated in control virus-infected cells during the 4-day culture. In marked contrast, demethylation was dramatically accelerated in NICD-expressing NPCs (Figures 1H and 1I). Another astrocyte-specific gene (*S100β*) promoter was also demethylated by expression of NICD in these cells (Figure S3). These results confirm that the activation of Notch signaling is sufficient to endow E11.5 NPCs with the ability to differentiate into astrocytes by inducing demethylation of astrocytic gene promoters.

Committed Neuronal Precursors and Young Neurons, Pregenerated from NPCs, Express Notch Ligands

It was previously shown that Notch signaling is activated in cells adjacent to MASH1/NEUROGENIN (NGN)-expressing cells in the fetal ventricular zones (VZs) (Tokunaga et al., 2004), and that NGNs induce expression of the Notch ligand, DELTA LIKE 1 (DLL1), in neuronal precursors (Castro et al., 2006). Thus, to obtain direct evidence for an interaction between NGN-expressing cells and NPCs through Notch signaling in vivo, we examined spatiotemporal patterning of Notch activation and expression of its ligand in the mouse embryonic forebrain. We observed that Notch signal-activated cells existed in the cortical VZ at E11.5

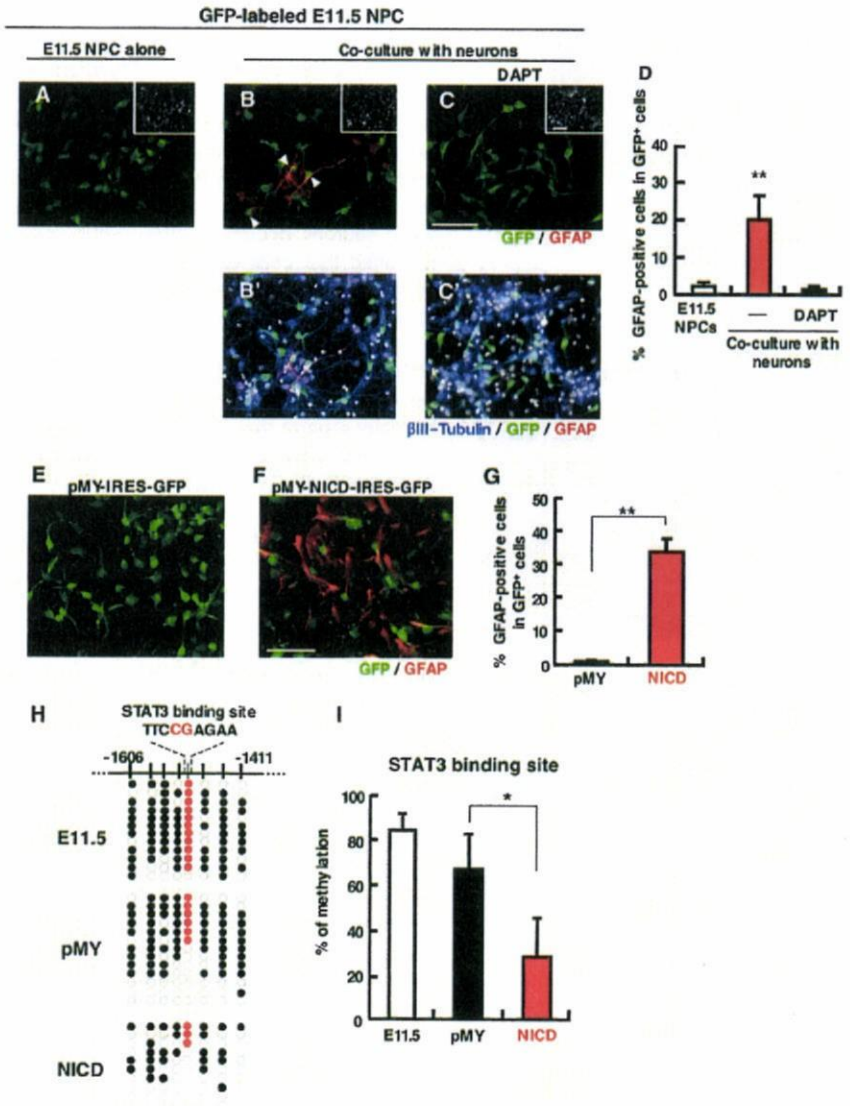

Figure 1. Pregenerated Neurons Potentiate NPCs to Differentiate into Astrocytes via Notch Signal Activation

(A and B) E11.5 NPCs labeled with GFP were cultured alone (A) or with embryonic cortical neurons (B) in the presence of LIF (80 ng/ml) for 4 days.

(C) Coculture as in (B) was performed in the presence of the γ-secretase inhibitor, N-[N-(3,5-Difluorophenacetyl-L-Alanyl)]-S-phenylglycine t-butyl ester (DAPT). After 4 days, the cells in (A)–(C) were stained with antibodies against GFP (green) and GFAP (red). Insets: H33258 nuclear staining of each field. (B′ and C′) β III-tubulin (blue) and H33258 nuclear staining (gray) are superimposed on (B) and (C). Scale bar = 50 μm.

(D) GFAP-positive astrocytes in GFP-positive cells were quantified. Data represent means ± SD (n = 3). Statistical significance was evaluated by one-way ANOVA (**$p < 0.01$).

(E and F) E11.5 NPCs were infected with retroviruses engineered to express GFP alone (E) or GFP together with NICD (F), cultured for 24 hr in the presence of bFGF, and then stimulated with LIF (80 ng/ml) for a further 3 days to induce astrocyte differentiation. The cells in (E) and (F) were stained with antibodies against GFP (green) and GFAP (red). Scale bar = 50 μm.

(G) GFAP-positive astrocytes in GFP control (pMY) and GFP-NICD-expressing cells were quantified. Data are shown as means ± SD. Statistical significance was examined by the Student t test (**$p < 0.01$).

(H) E11.5 NPCs were infected with GFP control (pMY) and GFP-NICD-expressing retroviruses, and were cultured for 4 days with bFGF. After cell sorting based on GFP fluorescence, genomic DNA was extracted from the cells, and the methylation status of the STAT3 binding site and other CpG sites around this sequence in the *gfap* promoter was examined by bisulfite sequencing. "E11.5" indicates the result obtained for freshly prepared NPCs from forebrain at E11.5. Closed and open circles indicate methylated and unmethylated CpG sites, respectively.

(I) Methylation frequency of the CpG site within the STAT3 binding sequence in the *gfap* promoter. Data are shown as means ± SD (n = 3). Statistical significance was examined by the Student t test (*$p < 0.05$).

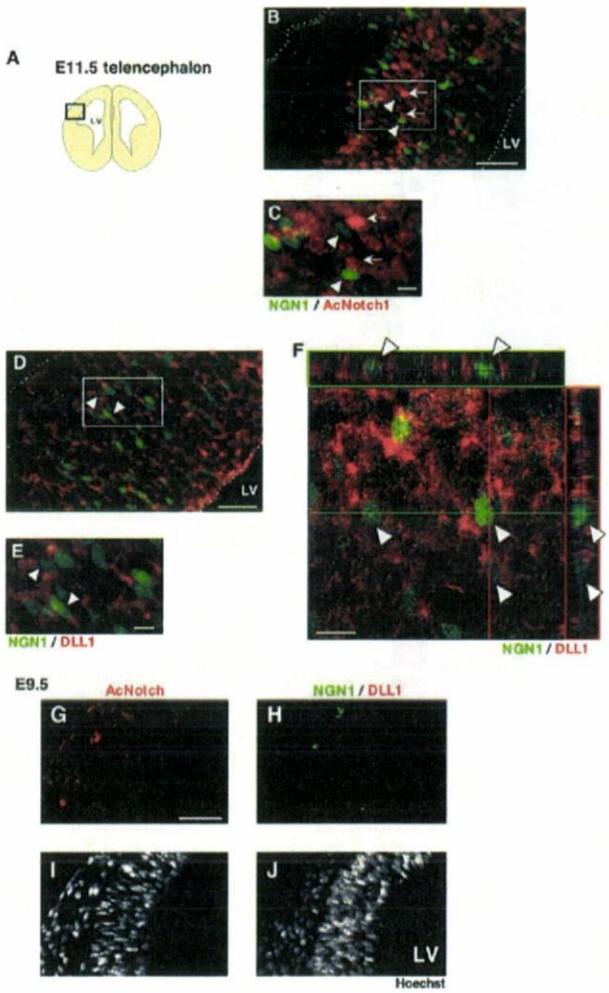

Figure 2. NGN1-Postive Cells Expressing DLL1 and Notch Signal-Activated Cells Are Mutually Exclusive

(A and B) E11.5 forebrain sections (B) from the region illustrated in (A) were immunostained with antibodies against activated Notch (AcNotch, red) and NGN1 (green). Arrows (AcNotch) and arrowheads (NGN1) indicate representatives of each cell type. Notch activation and NGN1 expression were mutually exclusive in these cells. LV, lateral ventricle. Scale bar = 20 μm.

(C) High-magnification view of boxed area in (B). Scale bar = 10 μm.

(D) E11.5 forebrain sections were stained with antibodies against NGN1 (NGN1, green) and DLL1 (DLL1, red). DLL1 was expressed in NGN1-positive differentiating neurons (arrowheads in [D]–[F] mark representatives). Scale bar = 20 μm.

(E) High-magnification view of boxed area in (D). Scale bar = 10 μm.

(F) Coexpression of DLL1 and NGN1 in these cells was confirmed by three-dimensional digital imaging of a brain section immunostained as in (D). Scale bar = 10 μm.

(G and H) E9.5 forebrain sections (12 μm) were stained with antibodies against activated Notch (AcNotch, red) (G), or NGN1 (green) and DLL1 (red) (H). Scale bar = 50 μm.

(I and J) H33258 staining of nuclei of cells in (G) and (H), respectively. No Notch-activated or NGN1-positive cells were observed in VZ at E9.5. LV, lateral ventricle.

(Figures 2A–2C), but not yet at E9.5 (Figures 2G–2J). These results suggest that the timing of Notch signal activation coincides with the onset of demethylation of the *gfap* promoter STAT3 binding site in vivo. Notably, most of the Notch-activated NPCs appeared to be located adjacent to NGN1-expressing cells, and Notch activation and NGN1 expression were mutually exclusive in these cells (Figures 2A–2C). Since NGN1 is a proneural gene product, the expression of which is downregulated when neurons become mature (Schuurmans et al., 2004), we reasoned that cells expressing NGN1 at this stage are either committed neuronal precursors or neurons at very early stages of maturation (Kawaguchi et al., 2008). Furthermore, DLL1 and another Notch ligand, JAGGED1 (JAG1) (Tokunaga et al., 2004; Xue et al., 1999), were expressed in NGN1-expressing cells (Figures 2D–2F; Figures S4A–S4C), consistent with previous reports that *Dll1* is expressed in migrating committed neuronal daughters (intermediate progenitor and young neurons) (Henrique et al., 1995; Castro et al., 2006; Campos et al., 2001; Yoon et al., 2008; Kawaguchi et al., 2008). In agreement with these observations, we found that a significant number of NGN1-positive cells were also positive for T-box brain gene 2, a marker of intermediate progenitor cells (Figures S5A–S5C). On the other hand, Notch-activated NPCs appeared to be radial glial cells, as judged by their morphology through immunostaining with an anti-Nestin antibody (Figures S5D–S5L). Collectively, these data indicate that committed neuronal precursors and young neurons, pregenerated from NPCs, act as a trigger for activation of Notch signaling in adjacent residual NPCs at midgestation.

It should be noted that, although Notch signaling is activated in NPCs at E11.5 in vivo, these NPCs seemed not yet to have the potential to differentiate into GFAP-positive astrocytes when cultured in vitro (Figures 1A, 1C–1E, and 1G). This may be because Notch signal activation had not been underway for long enough to induce the demethylation of astrocytic gene promoters before the NPCs were transferred to in vitro culture, at which point the cell density became sparse compared with that in the brain, leading to insufficient Notch signal activation for the demethylation under these in vitro conditions.

Notch Activation Is Necessary for Astrocyte Differentiation

We next asked whether the Notch downstream molecule, CSL, is involved in Notch-induced demethylation of astrocytic gene promoters in NPCs. To address this, we used CSL-deficient mouse embryonic stem cells (mESCs) (Schroeder et al., 2003), since CSL-deficient embryos die at around E9.5 before neurogenesis in the telencephalon. As has been previously shown, mESC-derived NPCs recapitulate the sequential onset of neuronal and glial differentiation observed in vivo in these cultures (Shimozaki et al., 2005). As expected, at early times in suspension culture, mESC NPCs primarily differentiated into neurons under differentiation-culture conditions, even in the presence of LIF for 4 days (Figure 3A). After 2 weeks in suspension, wild-type (WT) mESC NPCs differentiated into GFAP-positive cells in response to LIF (Figure 3A). In CSL-deficient mESC NPCs, however, no astrocytic differentiation induced by LIF was observed, even after 2 weeks in suspension (Figure 3A). Consistent with these results, the hypermethylated status of

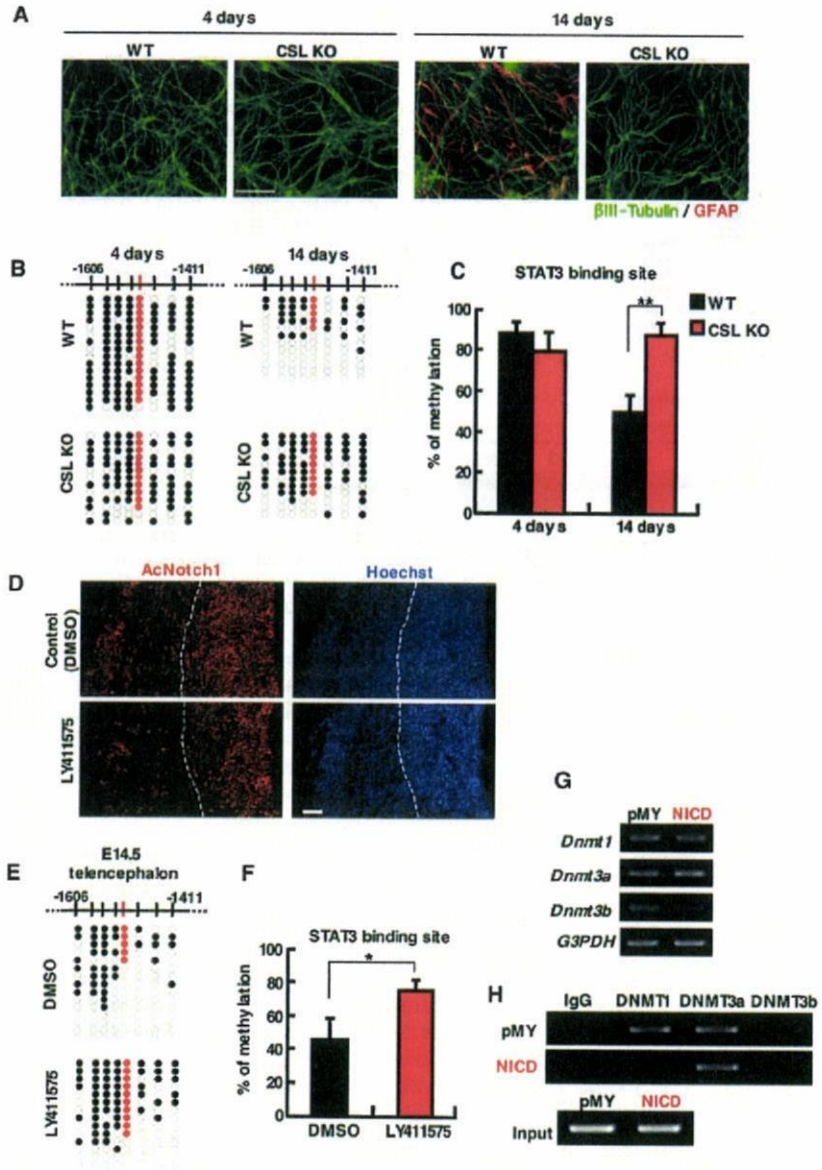

Figure 3. Requirement of CSL for Astrocytic Differentiation and Demethylation of *Gfap* Promoter of NPCs

(A) WT or CSL-deficient (CSL KO) mESCs were cultured in serum-free medium without LIF (neural spheroid, mESC-NPC culture) on poly-HEMA-coated dishes to make suspended aggregates. After 4 or 14 days, the aggregates were dissociated, seeded onto ornithine/fibronectin-coated dishes (monolayer culture) with LIF (80 ng/ml), and incubated for 4 days. Cells were stained with antibodies against a neuronal marker, β-III Tubulin (Tuj1, green), and GFAP (red). LIF-induced GFAP-positive astrocyte differentiation was observed in WT, but not in CSL-deficient mESCs, even after 14 days in suspension. Scale bar = 50 μm.

(B) Bisulfite sequencing results for the CpG site within the STAT3 recognition sequence (red) and other CpG sites around this sequence of the *gfap* promoter in WT and CSL-deficient mESC NPCs cultured as in (A). Each cell type was collected after 4 days in monolayer culture to extract genomic DNA. Closed and open circles indicate methylated and unmethylated CpG sites, respectively.

(C) Methylation frequency of the CpG site within the STAT3 binding sequence in the *gfap* promoter. Data are shown as means ± SD (n = 3). Statistical significance was examined by the Student t test (*$p < 0.05$).

(D) E14.5 forebrain sections of dimethyl sulfoxide (DMSO)- (upper panels) or LY411575 (lower panels)-treated embryonic mice were stained with antibodies against activated Notch (AcNotch in left panels, red). Hoechst staining indicates nuclei (right panels, blue). The white dotted line marks the boundary between the intermediate zone and VZ/SVZ in telencephalon. Scale bar = 50 μm.

(E) Bisulfite sequencing results for the CpG site within the STAT3 recognition sequence (red) and other CpG sites around this sequence of the *gfap* promoter in telencephalon of DMSO- or LY411575-treated embryos.

(F) Methylation frequency of the CpG site within the STAT3 binding sequence in the *gfap* promoter. Data are shown as means ± SD (n = 3). Statistical significance was examined by the Student t test (*$p < 0.05$).

(G) E11.5 NPCs were infected with GFP- or GFP-NICD-expressing virus and cultured for 4 days. After sorting of virus-infected cells based on GFP fluorescence, the expression level of each *Dnmt* gene was examined by RT-PCR.

(H) ChIP assay with specific antibodies for respective DNMTs from GFP- and GFP-NICD-expressing retrovirus-infected NPCs, cultured as in Figure 1G. Dissociation of DNMT1 from the *gfap* promoter was observed in response to NICD expression.

the *gfap* promoter STAT3 site was maintained in CSL-deficient mESC NPCs, compared with WT mESC NPCs (Figures 3B and 3C). Recently, it has been reported that CSL-deficient ESCs are defective in neural precursor generation (Lowell et al., 2006). However, we observed that NPCs can arise from CSL-deficient mESCs in our culture conditions, which are based on methods described previously (Shimozaki et al., 2005), as judged by Nestin or βIII-tubulin staining (Figure 3A and data not shown).

To determine whether the activation of Notch signaling is necessary for demethylation of the astrocyte-specific gene promoter in vivo, we administered the γ-secretase inhibitor, LY411575, to pregnant mice from 10.5 to 13.5 days postcoitum (dpc) and examined the activation of Notch signaling, by immunohistochemistry and by monitoring the methylation status of the *gfap* promoter in E14.5 embryonic telencephalon. As expected, the number of Notch signal-activated cells in the VZ of LY411575-treated embryos was significantly lower than that in control mice (Figure 3D). Moreover, many βIII-tubulin-positive neurons were observed in the VZ of LY411575-treated embryos compared with control mice, suggesting that the disruption of Notch signaling in NPCs leads to an overproduction of neurons

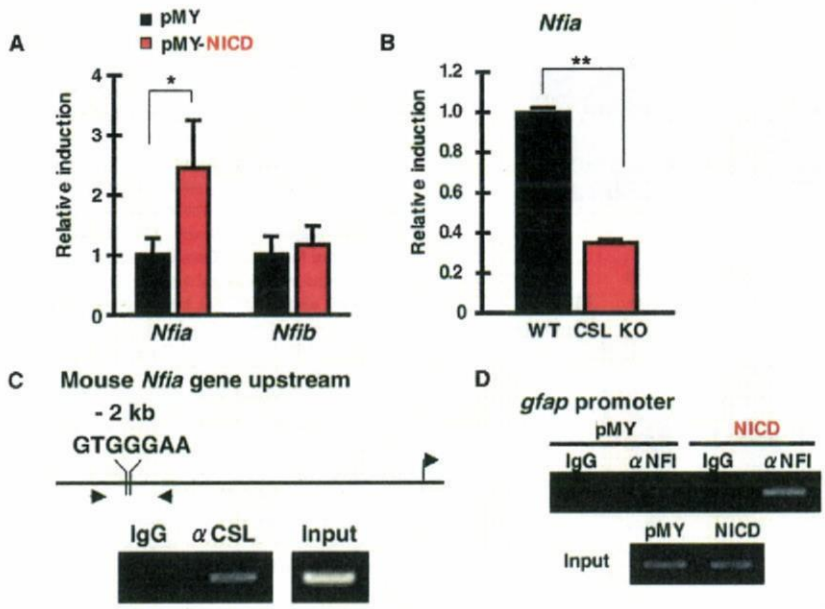

Figure 4. NFI Is a Downstream Molecule of Notch Signaling in NPCs

(A) E11.5 NPCs were infected with GFP- (pMY, closed bars) or GFP-NICD-expressing virus (NICD, red bars) and cultured for 4 days. After sorting of virus-infected cells based on GFP fluorescence, the expression level of *Nfia* and *Nfib* mRNAs was examined by real-time RT-PCR. Data are shown as means ± SD (n = 3). Statistical significance was examined by the Student t test (*$p < 0.05$).

(B) Expression level of *Nfia* mRNA in NPCs derived from ES cells cultured as in (A) (14 days) was examined by real-time RT-PCR. Data are shown as means ± SD (N = 3). Statistical significance was examined by the Student t test (**$p < 0.01$).

(C) ChIP assay of E11.5 NPCs with an antibody against CSL. Binding of CSL to a region containing a CSL cognate sequence located ~2 kb upstream of the *Nfia* transcriptional start site (arrow at right) was detected in E11.5 NPCs.

(D) ChIP assay with an anti-NFI antibody from GFP- and GFP-NICD-expressing retrovirus-infected NPCs cultured as in Figure 1G. Binding of NFI to the *gfap* promoter was observed in response to NICD expression.

(Figure S6A). Consistent with this reduction of Notch signal activation, *gfap* promoter methylation was much higher in the treated embryos than in the controls (Figures 3E and 3F). Furthermore, when we purified NPCs from E14.5 embryos of mice expressing an enhanced GFP (EGFP)transgene under the NPC marker *Sox2* gene promoter (D'Amour and Gage, 2003) by FACS sorting, we observed that the *gfap* promoter in cells from LY411575-treated embryos was hypermethylated compared with its status in control mice (Figures S6B and S6C). We conclude from these experiments that the activation of Notch signaling is prerequisite for demethylation of the astrocyte-specific *gfap* promoter both in vitro and in vivo.

Notch Activation Impairs the Association of Maintenance Methyltransferase with the *gfap* Promoter in NPCs

To establish which DNA methyltransferases (DNMTs) participate in NICD-induced demethylation of the *gfap* promoter, we next examined the expression levels of one maintenance (*Dnmt1*) and two de novo (*Dnmt3a* and *Dnmt3b*) methyltransferase genes by RT-PCR in control and NICD-expressing E11.5 NPCs. Surprisingly, we found no significant differences in *Dnmt* expression between the two cell populations, although *Dnmt3b* expression decreased slightly in NICD-expressing NPCs (Figure 3G). On the other hand, chromatin immunoprecipitation (ChIP) assays with specific antibodies against the three DNMTs revealed that DNMT1 and DNMT3a associated with the *gfap* promoter in the control NPCs (Figure 3H). DNMT1 dissociated from the promoter when Notch signaling was activated (Figure 3H), however, implying that its dissociation may be in part responsible for the Notch-induced demethylation. Moreover, NICD-induced demethylation of the *gfap* promoter was not observed in the absence of basic fibroblast growth factor (bFGF), which is essential for proliferation of NPCs. The proliferation rates of control and NICD-expressing virus-infected cells were similar, as judged by bromodeoxyuridine uptake in the presence of bFGF, ruling out the possibility that selective proliferation of NICD-expressing NPCs occurred (data not shown). Notch-induced demethylation of the astrocytic gene promoter is therefore apparently attributable to passive demethylation: maintenance methylation of genomic DNA, following DNA replication and cell division, fails due to DNMT1 dissociation from the promoter.

NFI Acts as a Critical Molecule Downstream of the Notch Signaling Pathway to Potentiate Astrocytic Differentiation of Midgestational NPCs

A recognition sequence for NFI (Gronostajski, 2000), which is known to play an important role in migration and differentiation of astrocyte precursors (Deneen et al., 2006), has been identified in the *gfap* promoter, and is conserved among human, rat, and mouse (Krohn et al., 1999). We thus next examined whether *Nfi*-family gene expression is upregulated by Notch activation, and found that the expression of *Nfia* indeed increased (Figure 4A). Moreover, its expression was reduced markedly in NPCs from CSL-deficient mESCs compared with that in NPCs from WT mESCs (Figure 4B). We also identified a consensus CSL-binding sequence ~2 kb upstream of the *Nfia* transcription start site, and binding of CSL to this region in NPCs was confirmed (Figure 4C). Furthermore, Notch activation led to binding of NFI to the *gfap* promoter (Figure 4D). To determine whether NFIA expression depends on the activation of Notch signaling, we examined NFIA expression by immunohistochemistry in the telencephalon of LY411575-treated embryos. The area of the VZ occupied by NFIA-positive cells was significantly reduced in LY411575-treated embryos (Figure S7), supporting the scenario that NFIA expression is controlled by the activation of Notch signaling in NPCs.

These results implied that NFI is involved in the Notch-induced potentiation of NPCs to differentiate precociously into astrocytes. To test this notion, E11.5 NPCs were infected with

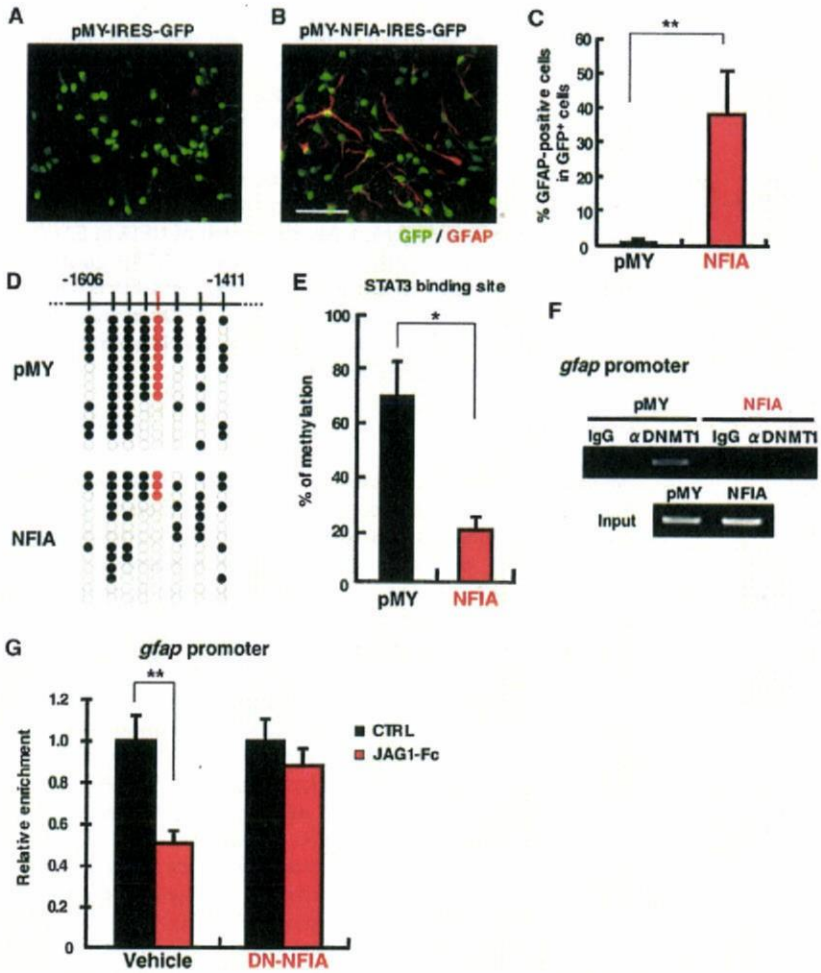

Figure 5. NFI Functions as a Critical Downstream Molecule Mediating Notch Signaling to Potentiate Astrocytic Differentiation of Midgestational NPCs

(A and B) E11.5 NPCs were infected with retroviruses engineered to express GFP alone (A) or GFP together with NFIA (B), cultured for 24 hr in the presence of bFGF, and then stimulated with LIF (80 ng/ml) for a further 3 days to induce astrocytic differentiation. The cells were stained with antibodies against GFP (green) and GFAP (red). Scale bar = 50 μm.

(C) GFAP-positive astrocytes in GFP control (pMY) and GFP-NFIA-expressing (NFIA) cells were quantified. Data are shown as means ± SD. Statistical significance was examined by the Student's t test (**$p < 0.01$).

(D) E11.5 NPCs were infected with GFP control (pMY) and GFP-NFIA-expressing (NFIA) retroviruses, and cultured for 4 days with bFGF. After cell sorting based on GFP fluorescence, genomic DNA was extracted, and the methylation status of the STAT3 binding site in the *gfap* promoter was examined by bisulfite sequencing. Closed and open circles indicate methylated and unmethylated CpG sites, respectively.

(E) Methylation frequency of the CpG site within the STAT3 binding sequence in the *gfap* promoter. Data are shown as means ± SD (N = 3). Statistical significance was examined by the Student t test (*$p < 0.05$).

(F) ChIP assay with a specific antibody for DNMT1 from GFP- and GFP-NFIA-expressing retrovirus-infected NPCs, cultured as in Figure 1G.

(G) E11.5 NPCs were infected with control and DN-NFIA-expressing lentiviruses, and cultured for 4 days with (JAG1-Fc) or without (CTRL) JAG1-Fc in the presence of bFGF. A ChIP assay was performed with a specific antibody for DNMT1 from control (Vehicle) and DN-NFIA-expressing (DN-NFIA) lentivirus-infected NPCs, cultured as in Figure 5F. For quantification, real-time PCR results using specific primers for the *gfap* promoter were indicated as the relative enrichment of DNMT1 compared with NPCs cultured without JAG1-Fc. Data are shown as means ± SD (N = 3). Statistical significance was evaluated by the Student t test (**$p < 0.01$).

retroviruses engineered to express NFIA, and cultured in the presence of LIF. A dramatic induction of GFAP-positive astrocytic differentiation ensued (Figures 5A–5C). As was the case for NICD, GFAP was not expressed in control or NFIA-expressing NPCs in the absence of LIF (data not shown). Furthermore, *gfap* promoter demethylation and DNMT1 dissociation from the promoter were both accelerated in NFIA-expressing NPCs (Figures 5D–5F), as they were in NICD-expressing NPCs. These results prompted us to hypothesize that NFIA is necessary for the Notch-induced dissociation of DNMT1 from the *gfap* promoter. To answer this question, control and dominant-negative NFIA (DN-NFIA)-expressing lentivirus-infected E11.5 NPCs were cultured with JAG1-Fc, a soluble form of the Notch ligand JAG1, for 4 days. We then performed ChIP assays to examine the association of DNMT1 with the *gfap* promoter. In control NPCs, JAG1-Fc treatment led to the dissociation of DNMT1 from the *gfap* promoter, as in the case of NICD expression (Figure 5G). In contrast, we found that dissociation was virtually inhibited in NPCs infected with DN-NFIA-expressing lentiviruses (Figure 5G). Thus, these results indicate that NFIA is prerequisite for the Notch-induced dissociation of DNMT1 from the *gfap* promoter in NPCs. It is noteworthy that a consensus NFI binding site is also present in the promoters of other astrocytic genes, including *S100β*, *aquaporin4*, and *clusterin* (Saadoun et al., 2005; Bachoo et al., 2004) (Figure S8A), and the anticipated binding of NFI to these promoter regions was indeed observed in NICD-expressing NPCs (Figure S8B). Furthermore, demethylation of particular CpG sites within the three promoters was induced in NFIA-expressing NPCs (Figures S9A–S9C). These findings suggest that NFIA acts as a critical molecule downstream of the Notch signaling pathway to potentiate astrocytic differentiation of midgestational NPCs.

NFIA Is Necessary and Sufficient for NPCs to Acquire Astrocytic Potential In Vivo

Finally, we asked whether NFIA indeed plays a critical role in the acquisition of astrocytic potential by NPCs in vivo. To this end, we first stimulated E14.5 NPCs from WT and NFIA-deficient mice with LIF to induce astrocyte differentiation. Since E14.5 NPCs have normally already gained the potential to become

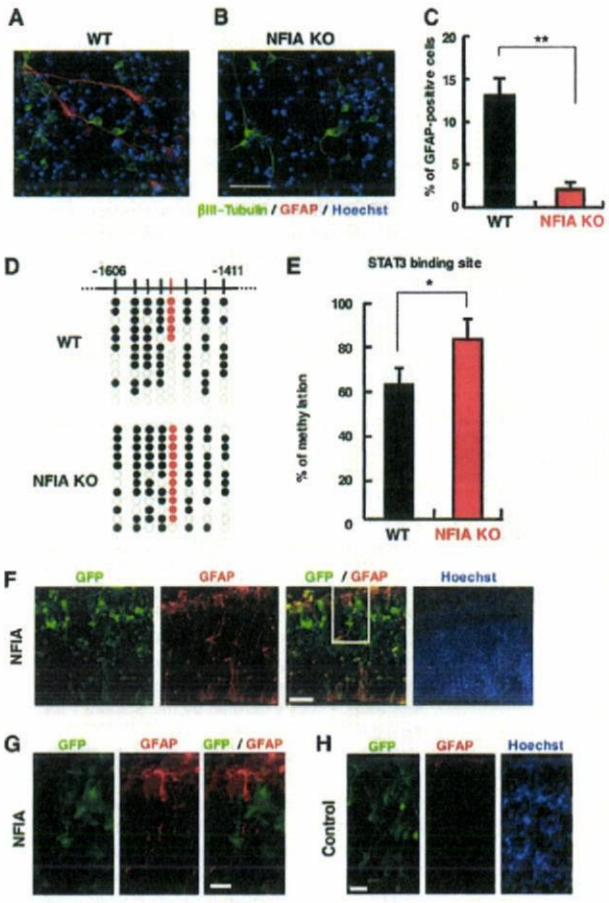

Figure 6. NFIA Is Necessary and Sufficient for the Expression of Astrocytic Potential by NPCs In Vivo

(A and B) NPCs prepared from E14.5 WT (A) or NFIA-deficient (NFIA-KO [B]) mouse telencephalons cultured in the presence of LIF (80 ng/ml) for 4 days to induce astrocytic differentiation. The cells were stained with antibodies against βIII-Tubulin (green) and GFAP (red), and with H33258 to identify nuclei (blue). Scale bar = 50 μm.

(C) GFAP-positive astrocytes in total cells were quantified. Data are shown as means ± SD (n = 3). Statistical significance was evaluated by the Student t test (**$p < 0.01$).

(D) Bisulfite sequencing results for the CpG site within the STAT3 recognition sequence (red) and other CpG sites around this sequence of the *gfap* promoter in telencephalon of WT or NFIA-deficient (NFIA-KO) mouse embryos. Closed and open circles indicate methylated and unmethylated CpG sites, respectively.

(E) Methylation frequency of the CpG site within the STAT3 binding sequence in the *gfap* promoter. Data are shown as means ± SD (n = 3). Statistical significance was examined by the Student t test (*$p < 0.05$).

(F–H) E14.5 forebrain sections of mice expressing GFP (H) and NFIA-GFP (F and G) from plasmids introduced by exo utero electroporation at E11.5 were stained with antibodies against GFP (green) and GFAP (red). Scale bars indicate 50 μm (F) or 20 μm (G and H). (G) High-magnification view of boxed area in (F). Hoechst staining indicates nuclei (blue).

GFAP-positive astrocytes in response to LIF, we observed astrocyte differentiation in the WT NPC culture. In marked contrast, almost no GFAP-positive cells were observed in NFIA-deficient NPCs. Moreover, the *gfap* promoter was significantly more highly methylated in E14.5 NFIA-deficient telencephalons than it was in those of WT litters (Figures 6D and 6E), even though Notch signal was clearly activated in the NFIA-deficient brain (Figure S10). These results indicate that NFIA is indispensable for the Notch signal-induced demethylation of astrocytic gene promoters during brain development.

Using exo utero electroporation, we next examined whether NFIA expression is sufficient for the induction of astrocyte differentiation in the telencephalon. Misexpression of NFIA in E11.5 telencephalon led to precocious generation of GFAP-positive cells at E14.5 (Figures 6F and 6G), indicating that NFIA is sufficient for the production of astrocytes from NPCs in vivo. We suggest that NFIA plays a decisive role in the Notch-induced acquisition of astrocytic potential by NPCs.

DISCUSSION

We have shown in the present study that committed neuronal precursors and young neurons derived from NPCs confer astrocytic differentiation potential on remaining NPCs through Notch signal-induced demethylation of astrocyte-specific gene promoters (Figure 7). The demethylation process is mediated by Notch-induced NFIA, the binding of which to astrocytic gene promoters leads to dissociation of DNMT1 from the promoters. This does not imply that the activation of Notch signaling alone is sufficient for NPCs to differentiate into astrocytes. It potentiates the process, but signals from astrocyte-inducing cytokines are still required to induce differentiation. All members of the IL-6 cytokine family, to which LIF and CT-1 belong, induce GFAP-positive astrocytic differentiation of NPCs by activating STAT1 and/or STAT3 (He et al., 2005; Barnabe-Heider et al., 2005). However, since STAT1 and STAT3 are not capable of binding to methylated cognate sequences (Fan et al., 2005; Takizawa et al., 2001), astrocyte-specific gene promoters must first become demethylated to enable IL-6 cytokines to induce differentiation.

Here, we have shown that committed neuronal precursors and young neurons pregenerated from NPCs express Notch ligands, and provide a feedback signal to Notch-expressing residual NPCs, to acquire astrocyte differentiation potential. In this context, Yoon et al. (2008) have shown recently that the expression of *Dll1* and its critical regulator, *Mindbomb*-1 (*Mib-1*), is restricted to migrating premature neurons and newborn neurons, and that *Mib-1*-expressing neuronal daughters transmit the Notch signal to neighboring NPCs. Moreover, *Mib-1* conditional mutant mice display a complete abrogation of Notch activation, which leads to impairment of NPC maintenance. Together with our results, these data suggest that Notch ligand-expressing, neuronally committed cells are an important cellular source of the Notch signal in development. Such a mechanism would provide an unanticipated level of crosstalk between these different developing cellular populations, and ensure that astrocytes begin to appear only after sufficient numbers of neurons have been generated.

Although Notch signaling clearly enhances astrocyte differentiation, the molecular mechanisms by which it activates glial gene expression have been far from clear. Our results suggest that NFI is one of the downstream target genes of the Notch signaling pathway, and plays a critical role in the Notch-induced

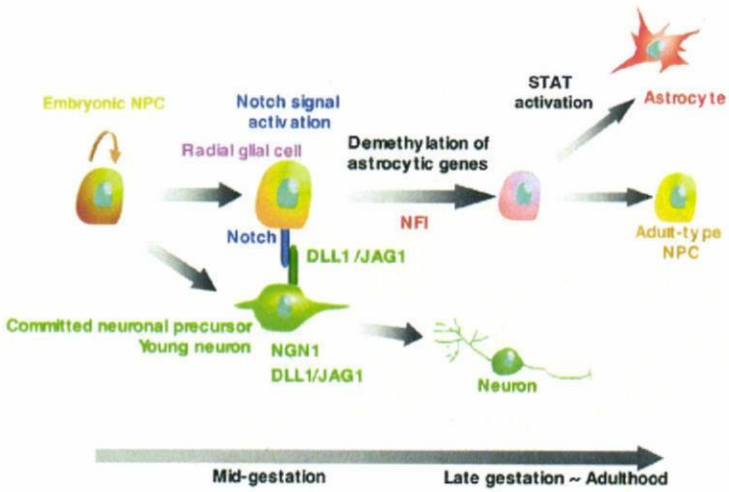

Figure 7. Schematic Representation of Notch Activation-Induced Potentiation of NPCs to Differentiate into Astrocytes and Sequential Changes in the Differentiation Potential of NPCs during Brain Development

At midgestation, an NPC divides asymmetrically and generates a committed neuronal precursor and another NPC (radial glial cells). The committed neuronal precursors and young neurons express Notch ligands and activate Notch signaling in neighboring NPCs, conferring astrocytic differentiation potential on NPCs through NFI expression, which leads to demethylation of astrocyte-specific gene promoters. When the NPCs receive a STAT-activating signal, they differentiate into astrocytes at late gestation. The NPCs eventually become multipotent adult-type NPCs.

acquisition of astrocyte differentiation potential by NPCs. Binding sites for NFI have indeed been identified, not only in the *gfap* promoter, but also in other astrocyte-specific gene promoters (Bachoo et al., 2004; Bisgrove et al., 2000; Gopalan et al., 2006; Saadoun et al., 2005), and *Nfia*$^{-/-}$ mice show reduced expression of these genes (Wong et al., 2007). It will therefore be intriguing to establish the methylation status of these gene promoters in *Nfia* mutant mice.

Since STAT1 and STAT3 are incapable of binding to methylated cognate sequences (Fan et al., 2005; Takizawa et al., 2001), the *gfap* promoter should already be demethylated in such cells as injury-induced reactive astrocytes, which are competent to express GFAP in response to inflammatory cytokines, including the IL-6 family. The existence of different morphological subtypes of astrocytes, such as fibrous and protoplasmic, has long been recognized, and protoplasmic astrocytes are generally GFAP negative (Vaughn and Pease, 1967; Mori and Leblond, 1969; Raff et al., 1984; Raff, 1989). Therefore, it remains unclear whether all astrocyte subtypes derived from NPCs in various brain regions require the Notch-induced demethylation of the *gfap* promoter reported here to become astrocytes.

Although DNA methyltransferases have been well studied biochemically, the molecular mechanism underlying active DNA demethylation is poorly understood, and the existence of DNA-demethylating enzymes is even debatable. A major outstanding question about the stepwise development of NPCs is how DNA methylation status is modulated to endow these precursor populations with glial competency. In this study, we have shown that demethylation of the *gfap* promoter, and dissociation of DNMT1 from the promoter, is caused by the expression of NICD or NFIA in NPCs in a sequential manner. These results suggest that the binding of NFIA to astrocytic gene promoters in Notch-activated NPCs protects the promoters from DNMT1, and hence that NFI plays a critical regulatory role in the epigenetic switch toward astrocytogenesis. We also suggest that demethylation of the *gfap* promoter is attributable to passive, replication-dependent demethylation. It has been reported previously that disruption of *Dnmt1* in NPCs leads to demethylation of astrocytic gene promoters and precocious astrogliogenesis, which suggests that *Dnmt1* is required for the maintenance methylation of astroglial marker genes in NPCs during the early developmental stage (Fan et al., 2005). Furthermore, virus-derived episomal vectors are demethylated at sites where transcription factors bind with high affinity (Hsieh, 1999; Lin et al., 2000), and replication-dependent demethylation of specific sites in *Xenopus* embryos is strongly stimulated by the transactivation domain of the triggering transcription factor (Matsuo et al., 1998). Thus, it is reasonable to hypothesize that passive demethylation is attributable to transcription factors that mask their cognate sites from DNMT1 action, although these and our findings do not yet permit a precise definition of the mechanism.

In summary, our present study offers a plausible explanation for the transitions that occur during the stepwise process of NPC fate specification, and we have suggested how committed neuronal precursors and young neurons might "unlock" nearby NPCs and allow them to differentiate into the next lineage: astrocytes. The activation of Notch signaling in midgestational NPCs induces demethylation of astrocyte-specific genes. Notch ligands are expressed in committed neuronal precursors and young neurons, and Notch-activated NPCs undergo promoter demethylation and acquire the ability to become astrocytes in response to astrocyte-inducing cytokines.

EXPERIMENTAL PROCEDURES

Cell Culture

E11.5 NPCs and embryonic neurons were cultured as described previously (Takizawa et al., 2001). Briefly, E14.5 cortical cells were cultured with bFGF and cytosine arabinoside for 4 days in the eight well chamber slides (4×10^4 cells per well). E11.5 NPCs labeled with EGFP (4×10^4 cells per well) were cultured with the embryonic neurons prepared as above, or alone (8×10^4 cells per well) in the chamber slides. Culturing of WT and CSL-deficient mESCs and induction of mESC NPCs were conducted as described previously (Shimozaki et al., 2005). To activate the Notch signaling pathway in Figure 5G, we used JAG1-Fc (500 ng/ml; R&D Systems).

Plasmids

To express NICD (Takizawa et al., 2003) and NFIA (Deneen et al., 2006), we used the retroviral vector pMY-IRES-GFP (Kitamura et al., 2003), which contains an IRES-GFP cassette that allows identification of transduced cells.

As DN-NFIA, we used the DNA binding domain of NFIA (NFIA-DBD) cloned by PCR from mNFIA cDNA. The NFIA-DBD was cloned into the lentiviral vector (Lois et al., 2002).

Immunostaining

All antibodies for immunostaining in this study and the procedures are descried in Supplemental Experimental Procedures.

LY411575 γ-Secretase Inhibitor Treatment

Pregnant mice were orally dosed with either 1 mg/kg LY411575 (Hyde et al., 2006) or vehicle (dimethyl sulfoxide in sunflower oil) once a day from 10.5 to 13.5 dpc. Twenty-four hours after the last injection at 13.5 dpc, the embryos at E14.5 were obtained for subsequent immunohistochemical analyses.

Bisulfite Sequencing

Cells expressing GFP alone, or GFP together with NICD or NFIA, were isolated by FACSVantage (BD Biosciences), and their genomic DNAs were then extracted. Bisulfite genomic sequencing was performed essentially, as previously described (Takizawa et al., 2001). Specific DNA fragments were amplified by PCR using primers described previously (Takizawa et al., 2001). The PCR products were cloned into pT7Blue vector (Novagen), and 10–16 clones randomly picked from each of three independent PCR amplifications were sequenced.

ChIP Assay

ChIP assays were performed as described previously (Takizawa et al., 2001). Coimmunoprecipitated DNA was used as a template for PCR with primers, the sequences of which are available upon request. Antibodies used for the ChIP assay were mouse anti-CSL (Institute of Immunology) and rabbit anti-NFI (Santa Cruz Biotechonoly), -DNMT1, -DNMT3a, and -DNMT3b (Abcam).

In Vivo Electroporation

Embryonic exo utero surgery and electroporation were performed as described previously (Muneoka et al., 1986; Saito and Nakatsuji, 2001). DNA solutions (pMYs or pMYs-*Nfia*, 2 mg/ml in PBS containing FAST Green) were injected into the lateral ventricle of E11.5 telencephalons. Electronic pulses of 28 V (50 ms) were charged six times at 950-ms intervals using a square-pulse electroporator (CUY21EDIT; Nepa Gene Company).

SUPPLEMENTAL DATA

Supplemental Data include Supplemental Experimental Procedures and ten figures and can be found with this article online at http://www.cell.com/developmental-cell/supplemental/S1534-5807(09)00002-1/.

ACKNOWLEDGMENTS

We thank T. Honjo (Kyoto University) for CSL-deficient ES cells, Y.E. Sun (University of California, Los Angeles) for *Dll3* cDNA, T. Kitamura (University of Tokyo) for pMY vector and Plat-E cells, and F.H. Gage (Salk Institute) for the SOX2-EGFP mouse. We appreciate Y. Bessho and T. Matsui for valuable discussions. We wish to thank the members of our laboratories, in particular I. Nobuhisa, for technical suggestions. We also thank I. Smith for helpful comments and critical reading of the manuscript. We are very grateful to M. Ueda for excellent secretarial assistance. Many thanks to N. Namihira for technical help. This work has been supported by a Grant-in-Aid for Young Scientists, a Grant-in-Aid for Scientific Research on priority areas, the NAIST Global COE Program (Frontier Biosciences: Strategies for Survival and Adaptation in a Changing Global Environment), Kumamoto University COE Program (Cell Fate Regulation Research and Education Unit) from the Ministry of Education, Culture, Sports, Science, and Technology (MEXT) of Japan, by CREST from Japan Science and Technology Agency, and by the Nakajima Foundation and the Uehara Memorial Foundation.

Received: June 30, 2008
Revised: December 1, 2008
Accepted: December 30, 2008
Published: February 16, 2009

REFERENCES

Androutsellis-Theotokis, A., Leker, R.R., Soldner, F., Hoeppner, D.J., Ravin, R., Poser, S.W., Rueger, M.A., Bae, S.K., Kittappa, R., and McKay, R.D. (2006). Notch signalling regulates stem cell numbers in vitro and in vivo. Nature *442*, 823–826.

Bachoo, R.M., Kim, R.S., Ligon, K.L., Maher, E.A., Brennan, C., Billings, N., Chan, S., Li, C., Rowitch, D.H., Wong, W.H., and DePinho, R.A. (2004). Molecular diversity of astrocytes with implications for neurological disorders. Proc. Natl. Acad. Sci. USA *101*, 8384–8389.

Barnabe-Heider, F., Wasylnka, J.A., Fernandes, K.J., Porsche, C., Sendtner, M., Kaplan, D.R., and Miller, F.D. (2005). Evidence that embryonic neurons regulate the onset of cortical gliogenesis via cardiotrophin-1. Neuron *48*, 253–265.

Bertrand, N., Castro, D.S., and Guillemot, F. (2002). Proneural genes and the specification of neural cell types. Nat. Rev. Neurosci. *3*, 517–530.

Bisgrove, D.A., Monckton, E.A., Packer, M., and Godbout, R. (2000). Regulation of brain fatty acid-binding protein expression by differential phosphorylation of nuclear factor I in malignant glioma cell lines. J. Biol. Chem. *275*, 30668–30676.

Campos, L.S., Duarte, A.J., Branco, T., and Henrique, D. (2001). mDll1 and mDll3 expression in the developing mouse brain: role in the establishment of the early cortex. J. Neurosci. Res. *64*, 590–598.

Castro, D.S., Skowronska-Krawczyk, D., Armant, O., Donaldson, I.J., Parras, C., Hunt, C., Critchley, J.A., Nguyen, L., Gossler, A., Gottgens, B., et al. (2006). Proneural bHLH and Brn proteins coregulate a neurogenic program through cooperative binding to a conserved DNA motif. Dev. Cell *11*, 831–844.

Cebolla, B., and Vallejo, M. (2006). Nuclear factor-I regulates glial fibrillary acidic protein gene expression in astrocytes differentiated from cortical precursor cells. J. Neurochem. *97*, 1057–1070.

das Neves, L., Duchala, C.S., Tolentino-Silva, F., Haxhiu, M.A., Colmenares, C., Macklin, W.B., Campbell, C.E., Butz, K.G., and Gronostajski, R.M. (1999). Disruption of the murine nuclear factor I-A gene (Nfia) results in perinatal lethality, hydrocephalus, and agenesis of the corpus callosum. Proc. Natl. Acad. Sci. USA *96*, 11946–11951.

D'Amour, K.A., and Gage, F.H. (2003). Genetic and functional differences between multipotent neural and pluripotent embryonic stem cells. Proc. Natl. Acad. Sci. USA *100* (*Suppl 1*), 11866–11872.

Deneen, B., Ho, R., Lukaszewicz, A., Hochstim, C.J., Gronostajski, R.M., and Anderson, D.J. (2006). The transcription factor NFIA controls the onset of gliogenesis in the developing spinal cord. Neuron *52*, 953–968.

Fan, G., Martinowich, K., Chin, M.H., He, F., Fouse, S.D., Hutnick, L., Hattori, D., Ge, W., Shen, Y., Wu, H., et al. (2005). DNA methylation controls the timing of astrogliogenesis through regulation of JAK-STAT signaling. Development *132*, 3345–3356.

Gopalan, S.M., Wilczynska, K.M., Konik, B.S., Bryan, L., and Kordula, T. (2006). Nuclear factor-1-X regulates astrocyte-specific expression of the alpha1-antichymotrypsin and glial fibrillary acidic protein genes. J. Biol. Chem. *281*, 13126–13133.

Grandbarbe, L., Bouissac, J., Rand, M., Hrabe de Angelis, M., Artavanis-Tsakonas, S., and Mohier, E. (2003). Delta-Notch signaling controls the generation of neurons/glia from neural stem cells in a stepwise process. Development *130*, 1391–1402.

Gronostajski, R.M. (2000). Roles of the NFI/CTF gene family in transcription and development. Gene *249*, 31–45.

He, F., Ge, W., Martinowich, K., Becker-Catania, S., Coskun, V., Zhu, W., Wu, H., Castro, D., Guillemot, F., Fan, G., et al. (2005). A positive autoregulatory loop of Jak-STAT signaling controls the onset of astrogliogenesis. Nat. Neurosci. *8*, 616–625.

Henrique, D., Adam, J., Myat, A., Chitnis, A., Lewis, J., and Ish-Horowicz, D. (1995). Expression of a delta homologue in prospective neurons in the chick. Nature *375*, 787–790.

Hsieh, C.L. (1999). Evidence that protein binding specifies sites of DNA demethylation. Mol. Cell. Biol. *19*, 46–56.

Hyde, L.A., McHugh, N.A., Chen, J., Zhang, Q., Manfra, D., Nomeir, A.A., Josien, H., Bara, T., Clader, J.W., Zhang, L., et al. (2006). Studies to investigate the in vivo therapeutic window of the gamma-secretase inhibitor N2-[(2S)-2-(3,5-difluorophenyl)-2-hydroxyethanoyl]-N1-[(7S)-5-methyl-6-oxo-6,7-dihydro-5H-dibenzo[b,d]azepin-7-yl]-L-alaninamide (LY411,575) in the CRND8 mouse. J. Pharmacol. Exp. Ther. *319*, 1133–1143.

Kato, H., Taniguchi, Y., Kurooka, H., Minoguchi, S., Sakai, T., Nomura-Okazaki, S., Tamura, K., and Honjo, T. (1997). Involvement of RBP-J in biological functions of mouse Notch1 and its derivatives. Development *124*, 4133–4141.

Kawaguchi, A., Ikawa, T., Kasukawa, T., Ueda, H.R., Kurimoto, K., Saitou, M., and Matsuzaki, F. (2008). Single-cell gene profiling defines differential progenitor subclasses in mammalian neurogenesis. Development *135*, 3113–3124.

Kitamura, T., Koshino, Y., Shibata, F., Oki, T., Nakajima, H., Nosaka, T., and Kumagai, H. (2003). Retrovirus-mediated gene transfer and expression cloning: powerful tools in functional genomics. Exp. Hematol. *31*, 1007–1014.

Kohyama, J., Tokunaga, A., Fujita, Y., Miyoshi, H., Nagai, T., Miyawaki, A., Nakao, K., Matsuzaki, Y., and Okano, H. (2005). Visualization of spatiotemporal activation of Notch signaling: live monitoring and significance in neural development. Dev. Biol. *286*, 311–325.

Krohn, K., Rozovsky, I., Wals, P., Teter, B., Anderson, C.P., and Finch, C.E. (1999). Glial fibrillary acidic protein transcription responses to transforming growth factor-beta1 and interleukin-1beta are mediated by a nuclear factor-1-like site in the near-upstream promoter. J. Neurochem. *72*, 1353–1361.

Ladi, E., Nichols, J.T., Ge, W., Miyamoto, A., Yao, C., Yang, L.T., Boulter, J., Sun, Y.E., Kintner, C., and Weinmaster, G. (2005). The divergent DSL ligand Dll3 does not activate Notch signaling but cell autonomously attenuates signaling induced by other DSL ligands. J. Cell Biol. *170*, 983–992.

Lin, I.G., Tomzynski, T.J., Ou, Q., and Hsieh, C.L. (2000). Modulation of DNA binding protein affinity directly affects target site demethylation. Mol. Cell. Biol. *20*, 2343–2349.

Lois, C., Hong, E.J., Pease, S., Brown, E.J., and Baltimore, D. (2002). Germline transmission and tissue-specific expression of transgenes delivered by lentiviral vectors. Science *295*, 868–872.

Louvi, A., and Artavanis-Tsakonas, S. (2006). Notch signalling in vertebrate neural development. Nat. Rev. Neurosci. *7*, 93–102.

Lowell, S., Benchoua, A., Heavey, B., and Smith, A.G. (2006). Notch promotes neural lineage entry by pluripotent embryonic stem cells. PLoS Biol. *4*, e121.

Matsuo, K., Silke, J., Georgiev, O., Marti, P., Giovannini, N., and Rungger, D. (1998). An embryonic demethylation mechanism involving binding of transcription factors to replicating DNA. EMBO J. *17*, 1446–1453.

Mori, S., and Leblond, C.P. (1969). Electron microscopic features and proliferation of astrocytes in the corpus callosum of the rat. J. Comp. Neurol *137*, 197–225.

Muneoka, K., Wanek, N., and Bryant, S.V. (1986). Mouse embryos develop normally exo utero. J. Exp. Zool. *239*, 289–293.

Nye, J.S., and Kopan, R. (1995). Developmental signaling: vertebrate ligands for Notch. Curr. Biol. *5*, 966–969.

Raff, M.C. (1989). Glial cell diversification in the rat optic nerve. Science *243*, 1450–1455.

Raff, M.C., Abney, E.R., and Miller, R.H. (1984). Two glial cell lineages diverge prenatally in rat optic nerve. Dev. Biol. *106*, 53–60.

Saadoun, S., Papadopoulos, M.C., Watanabe, H., Yan, D., Manley, G.T., and Verkman, A.S. (2005). Involvement of aquaporin-4 in astroglial cell migration and glial scar formation. J. Cell Sci. *118*, 5691–5698.

Saito, T., and Nakatsuji, N. (2001). Efficient gene transfer into the embryonic mouse brain using in vivo electroporation. Dev. Biol. *240*, 237–246.

Schroeder, T., Fraser, S.T., Ogawa, M., Nishikawa, S., Oka, C., Bornkamm, G.W., Honjo, T., and Just, U. (2003). Recombination signal sequence-binding protein Jkappa alters mesodermal cell fate decisions by suppressing cardiomyogenesis. Proc. Natl. Acad. Sci. USA *100*, 4018–4023.

Schuurmans, C., Armant, O., Nieto, M., Stenman, J.M., Britz, O., Klenin, N., Brown, C., Langevin, L.M., Seibt, J., Tang, H., et al. (2004). Sequential phases of cortical specification involve neurogenin-dependent and -independent pathways. EMBO J. *23*, 2892–2902.

Shimozaki, K., Namihira, M., Nakashima, K., and Taga, T. (2005). Stage- and site-specific DNA demethylation during neural cell development from embryonic stem cells. J. Neurochem. *93*, 432–439.

Shu, T., Butz, K.G., Plachez, C., Gronostajski, R.M., and Richards, L.J. (2003). Abnormal development of forebrain midline glia and commissural projections in Nfia knock-out mice. J. Neurosci. *23*, 203–212.

Steele-Perkins, G., Plachez, C., Butz, K.G., Yang, G., Bachurski, C.J., Kinsman, S.L., Litwack, E.D., Richards, L.J., and Gronostajski, R.M. (2005). The transcription factor gene Nfib is essential for both lung maturation and brain development. Mol. Cell. Biol. *25*, 685–698.

Takizawa, T., Nakashima, K., Namihira, M., Ochiai, W., Uemura, A., Yanagisawa, M., Fujita, N., Nakao, M., and Taga, T. (2001). DNA methylation is a critical cell-intrinsic determinant of astrocyte differentiation in the fetal brain. Dev. Cell *1*, 749–758.

Takizawa, T., Ochiai, W., Nakashima, K., and Taga, T. (2003). Enhanced gene activation by Notch and BMP signaling cross-talk. Nucleic Acids Res. *31*, 5723–5731.

Temple, S. (2001). The development of neural stem cells. Nature *414*, 112–117.

Tokunaga, A., Kohyama, J., Yoshida, T., Nakao, K., Sawamoto, K., and Okano, H. (2004). Mapping spatio-temporal activation of Notch signaling during neurogenesis and gliogenesis in the developing mouse brain. J. Neurochem. *90*, 142–154.

Vaughn, J.E., and Pease, D.C. (1967). Electron microscopy of classically stained astrocytes. J. Comp. Neurol. *131*, 143–154.

Weinmaster, G. (1997). The ins and outs of notch signaling. Mol. Cell. Neurosci. *9*, 91–102.

Wong, Y.W., Schulze, C., Streichert, T., Gronostajski, R.M., Schachner, M., and Tilling, T. (2007). Gene expression analysis of nuclear factor I-A deficient mice indicates delayed brain maturation. Genome Biol. *8*, R72.

Xue, Y., Gao, X., Lindsell, C.E., Norton, C.R., Chang, B., Hicks, C., Gendron-Maguire, M., Rand, E.B., Weinmaster, G., and Gridley, T. (1999). Embryonic lethality and vascular defects in mice lacking the Notch ligand Jagged1. Hum. Mol. Genet. *8*, 723–730.

Yoon, K.J., Koo, B.K., Im, S.K., Jeong, H.W., Ghim, J., Kwon, M.C., Moon, J.S., Miyata, T., and Kong, Y.Y. (2008). Mind bomb 1-expressing intermediate progenitors generate notch signaling to maintain radial glial cells. Neuron *58*, 519–531.

Yoshimatsu, T., Kawaguchi, D., Oishi, K., Takeda, K., Akira, S., Masuyama, N., and Gotoh, Y. (2006). Non-cell-autonomous action of STAT3 in maintenance of neural precursor cells in the mouse neocortex. Development *133*, 2553–2563.